ELSEVIER

Tectonophysics 354 (2002) 25–48

TECTONOPHYSICS

www.elsevier.com/locate/tecto

# Thermotectonic evolution of the western fold-and-thrust belt, southern Uralides, Russia, as revealed by apatite fission track data

U.A. Glasmacher [a,*], G.A. Wagner [a], V.N. Puchkov [b]

[a] *Max-Planck-Institut für Kernphysik, P.O. Box 103980, D-69029 Heidelberg, Germany*
[b] *Ufimian Geoscience Center, Russian Academy of Sciences, Ufa, Russia*

Received 10 August 2001; accepted 17 May 2002

**Abstract**

The Uralides, a linear N–S trending Palaeozoic fold belt, reveals an intact, well-preserved orogen with a deep crustal root within a stable continental interior. In the western fold-and-thrust belt of the southern Uralides, Devonian to Carboniferous siliciclastic and carbonate rocks overlay Mesoproterozoic to Neoproterozoic sedimentary rocks. Deformation in the Devonian, Carboniferous and Permian caused thick-skinned tectonic features in the western and central parts of the western fold-and-thrust belt. A stack of several nappes characterizes the deformation in the eastern part. Along the E–W transect AC-TS'96 that crosses the western fold-and-thrust belt, apatite fission track data record various stages of the geodynamic evolution of the Uralide orogeny such as basin evolution during the Palaeozoic, synorogenic movements along major thrusts, synorogenic to postorogenic exhumation and a change in the regional stress field during the Upper Jurassic and Lower Cretaceous. The Palaeozoic sedimentary cover and the Neoproterozoic basement of the Ala-Tau anticlinorium never exceed the upper limit of the PAZ since the Devonian. A temperature gradient similar to the recent one (20 °C/km) would account for the FT data. Reactivation of the Neoproterozoic Zilmerdak thrust was time equivalent to the onset of the Devonian and Carboniferous collision-related deformation in the east. West-directed movement along the Tashli thrust occurred in the Lower Permian. The Devonian and Carboniferous exhumation path of the Neoproterozoic siliciclastic units of the Tirlyan synclinorium mirrors the onset of the Uralian orogeny, the emplacement of the Tirlyan nappe and the continuous west-directed compression. The five main tectonic segments Inzer Synclinorium, Beloretzk Terrane, Ala-Tau anticlinorium, Yamantau anticlinorium and Zilair synclinorium were exhumed one after another to a stable position in the crust between 290 and 230 Ma. Each segment has its own t–T path but the exhumation rate was nearly the same. Final denudation of the western fold-and-thrust belt and exhumation to the present surface probably began in Late Tertiary. In Jurassic and Cretaceous, south-directed movements along W–E trending normal faults indicate a change in the tectonic regime in the southern Uralides.


*Keywords:* Apatite fission track; Thermal history; Ural mountains; Uralian orogeny; Mesozoic evolution

## 1. Introduction

The Uralide orogen forms a linear N–S trending Palaeozoic fold-and-thrust belt that extends for more than 2000 km from the Arctic Ocean almost to the

* Corresponding author. Tel.: +49-6221-516-321; fax: +49-6221-516-633.
*E-mail address:* ua.glasmacher@mpi-hd.mpg.de (U.A. Glasmacher).

0040-1951/02/$ - see front matter © 2002 Elsevier Science B.V. All rights reserved.
PII: S0040-1951(02)00286-X

Caspian Sea (Fig. 1). It resulted from the Palaeozoic two-stage collision of the East European Craton (EEC) with the Sibirian/Kazakhstanian continents and intervening accretion of island arc and micro-continental fragments (Hamilton, 1970; Zonenshain et al., 1984, 1990; Puchkov, 1988, 1993, 1997). The Main Uralian fault (MUF) is the major suture zone between the East European Craton to the west and the oceanic, island arc and continental terranes of Asia to the east (Zonenshain et al., 1984, 1990; Echtler and Hetzel, 1997). In comparison to other Palaeozoic orogens (e.g. the Variscides, Caledonides, etc.), the Uralide show a general bilateral symmetry with a western fold-and-thrust belt, a central magmatic arc zone (Magnitogorsk zone) and an eastern thrust belt with deep-reaching crustal shear zones (Berzin et al., 1996). However, unlike other Palaeozoic orogens that underwent postorogenic collapse and extension, the Uralide fold belt reveals an intact, well-preserved orogen with a deep crustal root within a stable continental interior (Echtler et al., 1996; Steer et al., 1998). The crustal root is interpreted as partially eclogitized lower crust (Döring and Götze, 1999; Leech, 2001). As the orogen is isostatically compensated and appears as though it has never departed far from this state, it represents an orogen that has escaped delamination of the lower crust and postorogenic extensional collapse (Giese, 2000; Leech, 2001). Thus, the Uralides are an exceptional example that allows the study of the synorogenic to postorogenic tectonothermal evolution of a Palaeozoic orogen. In the southern Urals, the Mesozoic to Cenozoic geological history is recorded by widespread sedimentary units in the Pre-Uralian Foredeep (PUF) and fluvial sediments along the drainage systems in the western fold-and-thrust belt. Based on the distribution of the fluvial sediments and the geomorphology, Borisevich (1992) argue for a Cretaceous uplift that caused the rise of the ranges and mountains above a ''Pre-Cretaceous peneplain''.

Seward et al. (1997) reported first apatite fission track data from a pilot project along the W–E transect URSEIS'95. They concluded very little differential movement within the footwall of the MUF since the Jurassic. Apatite FT data by Leech and Stockli (2000) indicate that the Maksyutov Complex (Fig. 1) was exhumed and cooled to 110 °C en masse in the Upper Carboniferous to Lower Permian (300 ± 25 Ma). Mesozoic slow cooling or reheating was followed by the final cooling in Cenozoic, which is interpreted as erosional degradation of the orogen.

In the frame of this paper, apatite fission track data are presented that aid constrain on the syndeformational to postdeformational history of the southern Uralides west of the MUF.

## 2. Regional geology

The most prominent feature of the western part of the southern Uralides is the Bashkirian Mega-anticlinorium (BMA), a broad NE and SSW plunging antiformal structure composed of Precambrian sedimentary strata (Figs. 1–3) (Kozlov, 1982). Mesoproterozoic to Neoproterozoic siliciclastic and carbonate units of the BMA are formed in terrestrial fluvial to shallow marine environment (Fig. 2) (Kozlov et al., 1989, 1995; Maslov et al., 1997). Upper Vendian polymict siliciclastic units are interpreted as flysch and molasse deposits of a Neoproterozoic orogenic event at the eastern margin of Baltica (Puchkov, 1997; Stroink et al., 1997; Giese et al., 1997, 1999; Glasmacher et al., 2001; Willner et al., 2001). In the west, the Tashli thrust separates the gently deformed Devonian to Permian strata (3000 m thickness) of the PUF from the folded structures of the BMA (Fig. 1). During the Permian, the PUF formed the western foreland basin to the Uralian orogeny with barrier reef complexes developed synchronously to prograding flysch sedimentation from the east. Lower Permian evaporites controlled the deformation and resulted in important ridge-like salt diapers.

The fold-and-thrust belt of the BMA is characterized by longitudinal regional-scale synclinal and anticlinal structures (from West to East: Ala-Tau anticlinorium, Inzer synclinorium, Yamantau anticlinorium) that are separated by important thrusts (Ala-Tau Th., Zilmerdak Th. and Avzyan Th.). In the North, East and South of the Ala-Tau anticlinorium, Vendian flysch deposits are overlain by Devonian to Carboniferous siliciclastic and carbonate units of about 2500 m thickness.

The Zuratkul Fault, the most prominent tectonic boundary in the BMA, can be traced south from the eastern limb of the Taratash complex approximately 300 km into the BMA (Fig. 1). It is the site of a major

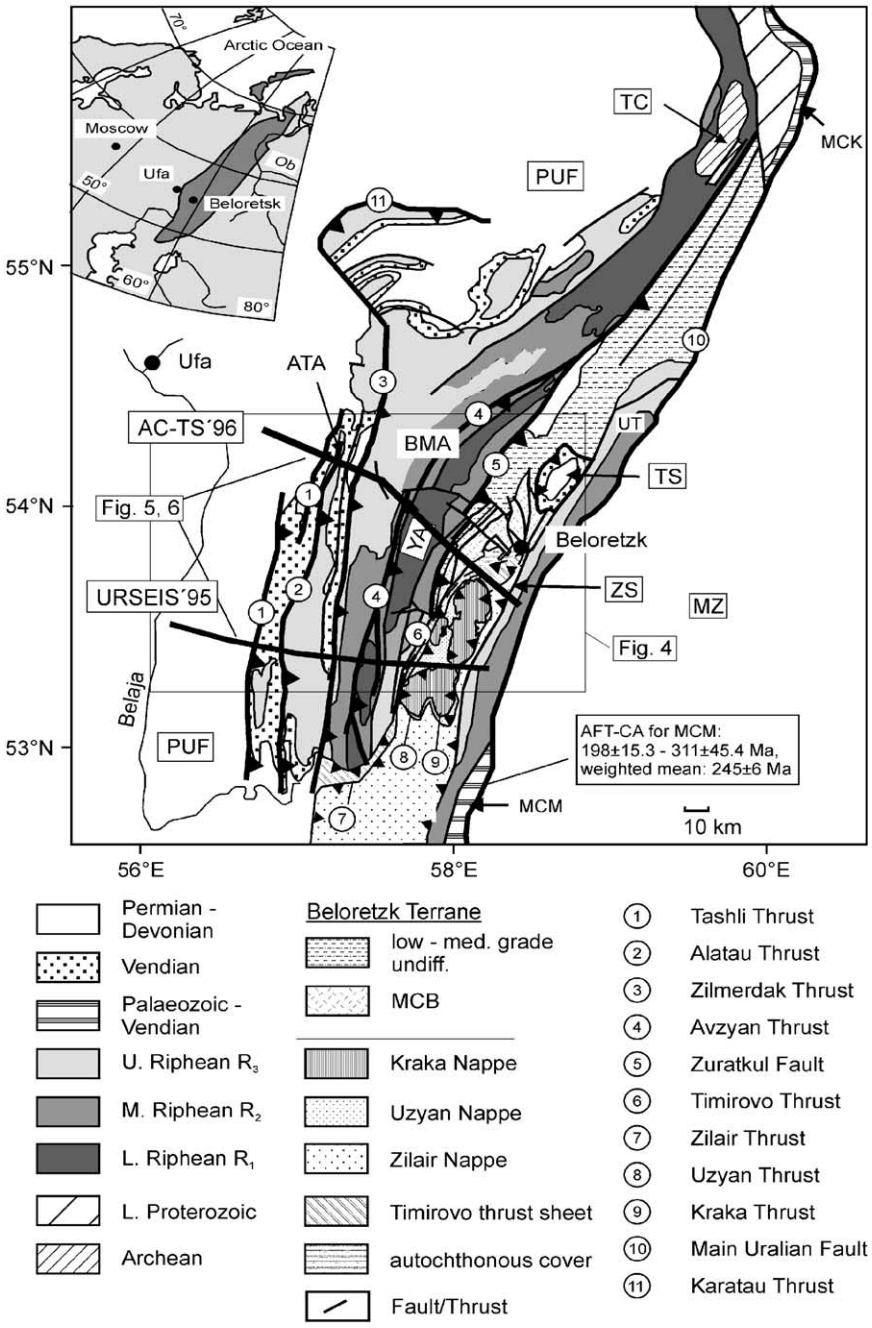


Fig. 1. Geological map of the western part of the southern Uralides (ATA: Ala-Tau anticlinorium, BMA: Bashkirian Mega anticlinorium, KC: Kraka complex, MCB: Metamorphic complex of Beloretzk, MCK: Metamorphic complex of Kurtinsky, MCM: Metamorphic complex of Maksyutov, PUF: Pre-Uralian Foredeep, TC: Taratash complex, TS: Tirlyan synclinorium, UT: Ural Tau, YA: Yamantau anticlinorium, ZS: Zilair synclinorium, MZ: Magnitogorsk zone). Apatite fission track central ages (AFT-CA) of the metamorphic complex of Maksyutov after Leech and Stockli (2000).

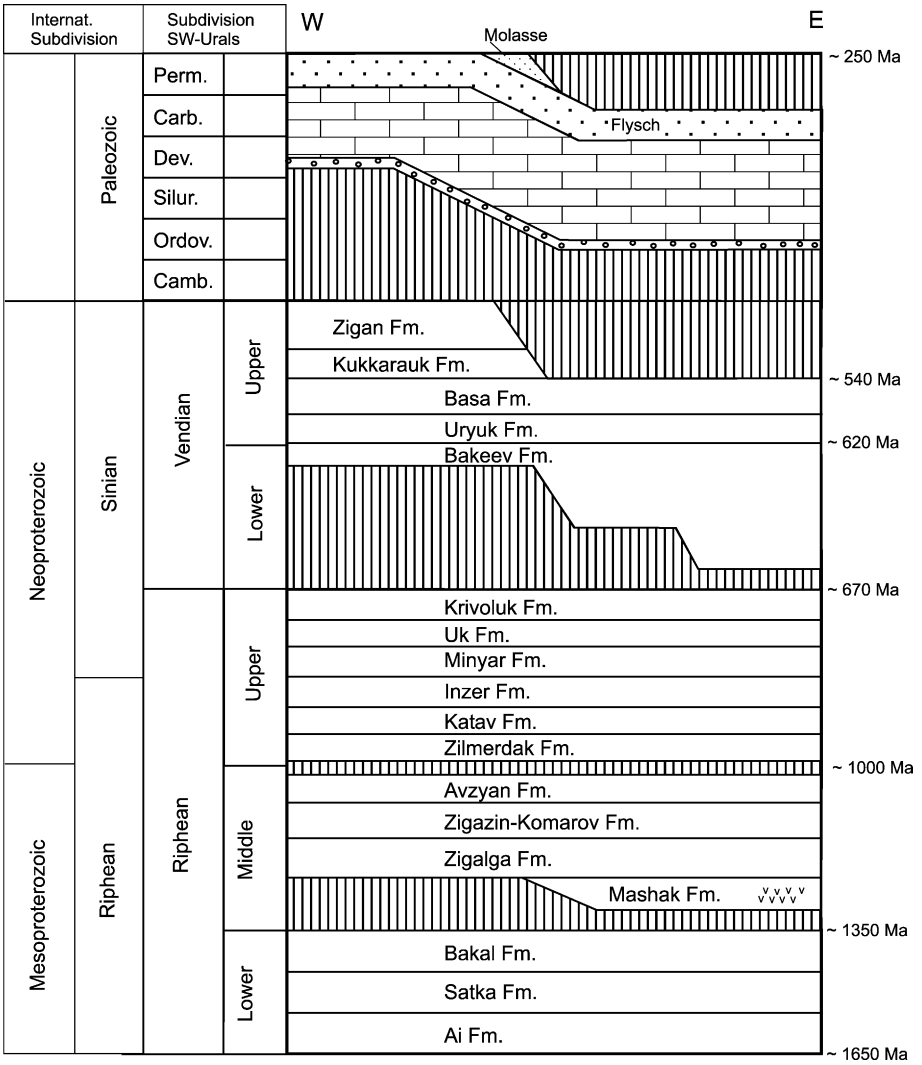


Fig. 2. Stratigraphic subdivision of the western fold-and-thrust belt, SW Uralides (according to Kozlov et al., 1995; Maslov et al., 1997 and international time scale after Haq and Eysinga van, 1998). Vertical hatching: hiatus, v: volcanic rocks.

structural and metamorphic break. Based on new structural, metamorphic and chronometric data, Glasmacher et al. (1999, 2001) reinterpreted the Zuratkul fault as a major terrane boundary that separates Neoproterozoic and Mesoproterozoic sedimentary units of the EEC from Mesoproterozoic low-grade to high-grade metamorphic units of the allochthonous Beloretzk Terrane.

East and south of the BMA, the Zilair synclinorium forms a SW-plunging, broad synform of Ordovician to Devonian siliciclastic and carbonate sedimentary rocks that unconformable overlie the Beloretzk Terrane (Figs. 1 and 3) (Giese et al., 1999; Glasmacher et al., 2001). Close to the unconformity at the AC-TS'96 transect, the Ordovician and Silurian sedimentary rocks are almost undeformed. Towards the east and along strike towards the south, the deformation increases. The first major thrust is located at the base of the Devonian limestones. East of this thrust, all rocks show NW-vergent folding and axial-planar cleavage. The late Devonian Zilair flysch that increase in thickness towards the south forms the entire core of

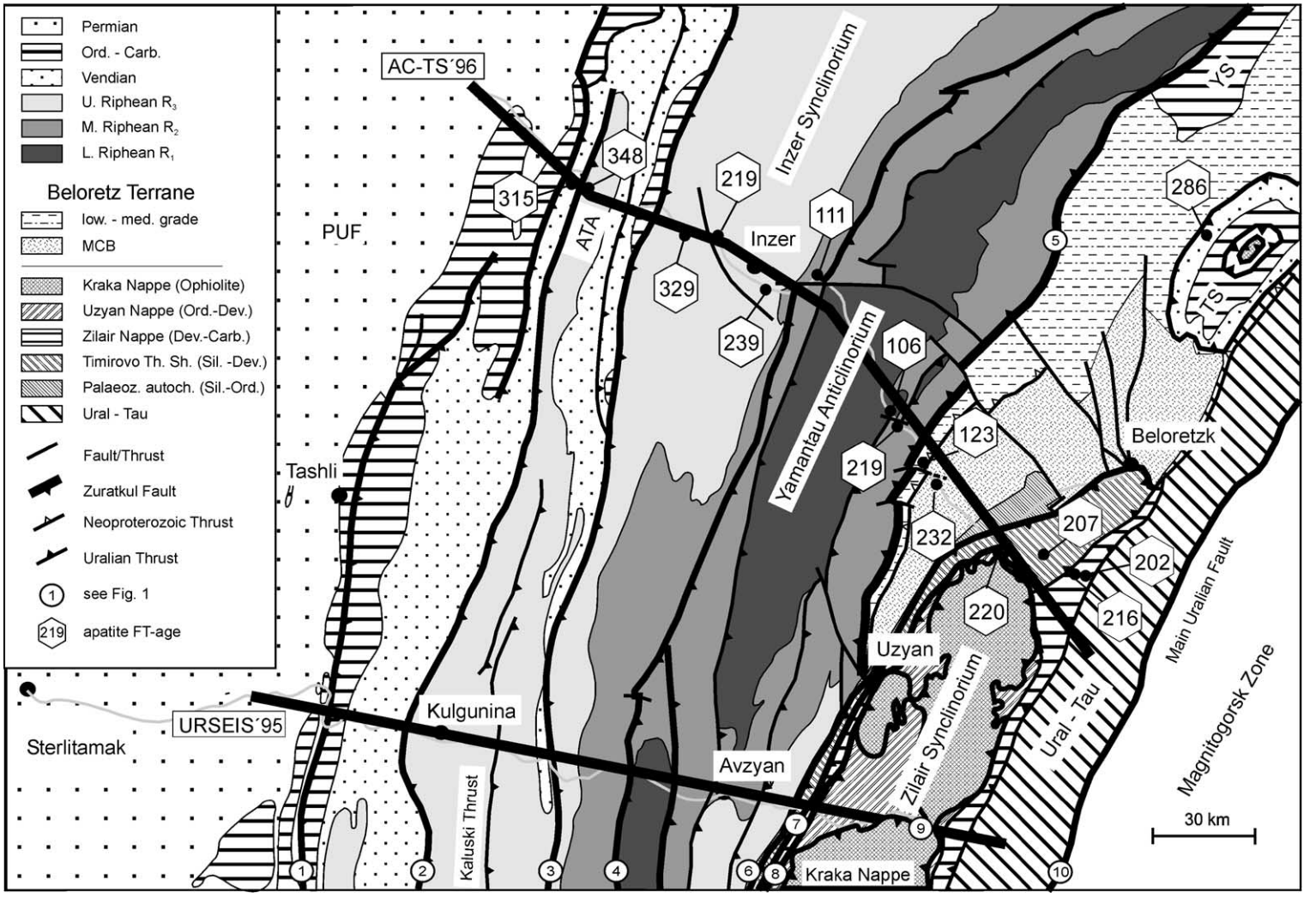


Fig. 3. Geological map of the investigated area (based on 1:200,000 scale map) (Giese et al., 1999).

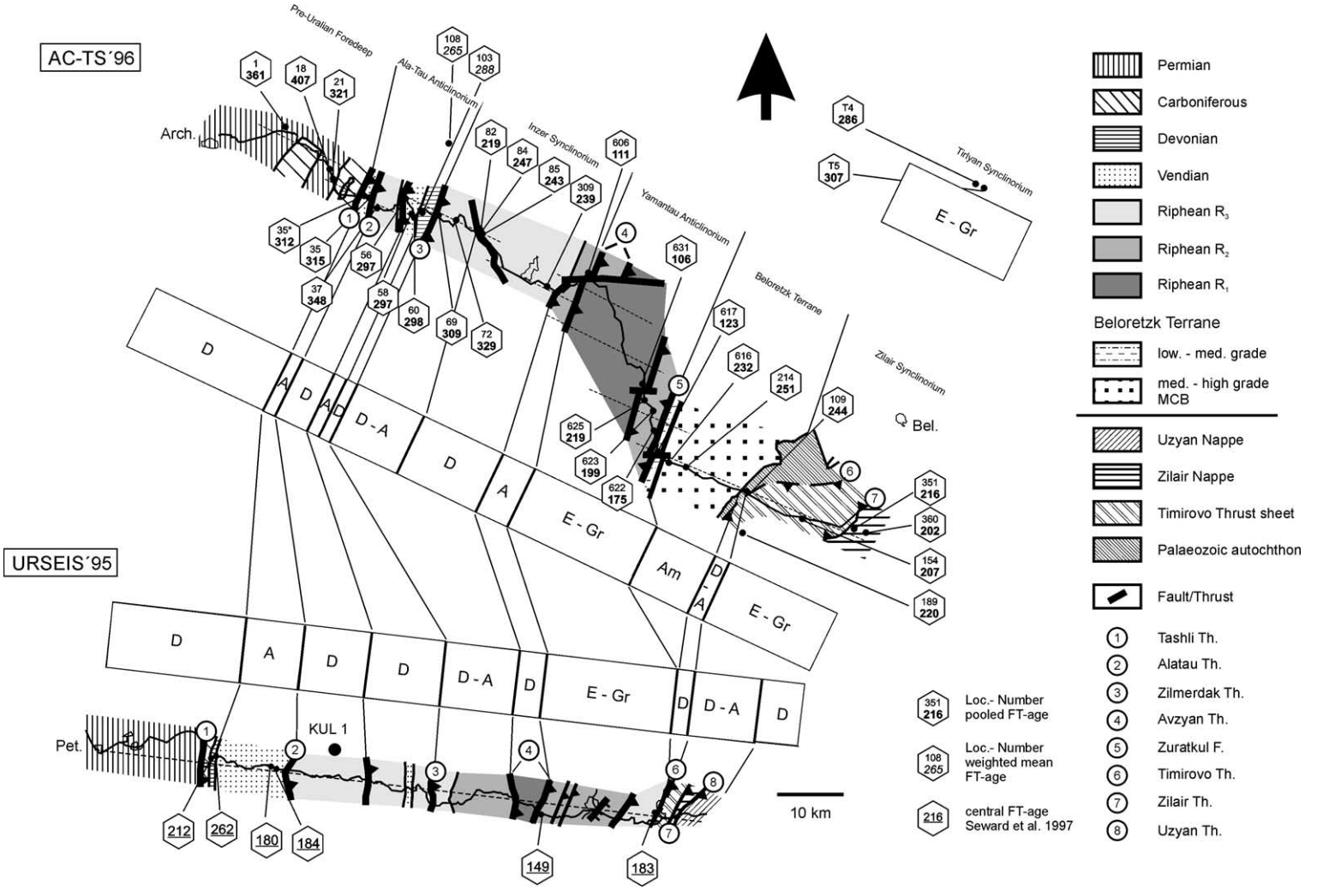


Fig. 4. Detailed geological maps of the area surrounding the sample location at the AC-TS'96 transect and the URSEIS'95 transect. Shown are also the sample locations, sample location numbers, apatite FT pooled ages and metamorphic grade determined by clay mineral crystallinity, vitrinite reflectance and conodont colour alteration index. Metamorphic data along the AC-TS'96 transect are described by Glasmacher et al. (1997) and Matenaar et al. (1999). Apatite FT central ages along the URSEIS'95 transect are taken from Seward et al. (1997). D: diagenesis, A: anchizone, E: epizone, Gr: greenschist facies, Am: amphibolite facies.

the synclinorium (Brown et al., 1996; Bastida et al., 1997; Puchkov, 1997). Brown et al. (1998) distinguished a Zilair nappe and a basal Timirovo thrust system (Fig. 3). The Zilair nappe is overthrusted by the Uzyan nappe, an imbricated unit of Ordovician to Devonian continental rise sedimentary rocks. Separated by a basal melange, the Kraka ophiolite complex, a nappe of unknown age, overlies the Uzyan nappe.

Clay mineral crystallinity, vitrinite reflectance and conodont colour alteration index were used to determine the thermal overprint of the Palaeozoic and Precambrian shales, slates and limestones along the AC-TS'96 and the URSEIS'95 transects (Fig. 4) (Glasmacher et al., 1997; Matenaar et al., 1999). Diagenetic to anchizonal grade was reached in the Pre-Uralian Foredeep, the Ala-Tau anticline, the Inzer synclinorium and the Zilair synclinorium, with changes related to the major thrust faults. In the Zilair synclinorium, the increase in metamorphic grade is accompanied by an increase of the intensity of cleavage. The Yamantau anticlinorium exceeds epizonal conditions.

The Palaeozoic geodynamic evolution of the western fold-and-thrust belt of the southern Uralides can be envisaged schematically as in Fig. 5 (Giese, 2000). The Palaeozoic shelf platform of the EEC is underlain by an outboard high-level metamorphic block, which finally consolidated during the Neoproterozoic orogeny (Fig. 5A) (Glasmacher et al., 1999, 2001). Towards the interior of the EEC, Palaeozoic shelf sedimentary rocks overlie a Riphean rift basin containing up to 15,000 m thick sedimentary units (Fig. 2). The onset of Uralian collision-related deformation is generally accepted to have taken place during Middle to Late Devonian times (Fig. 5B) (Brown et

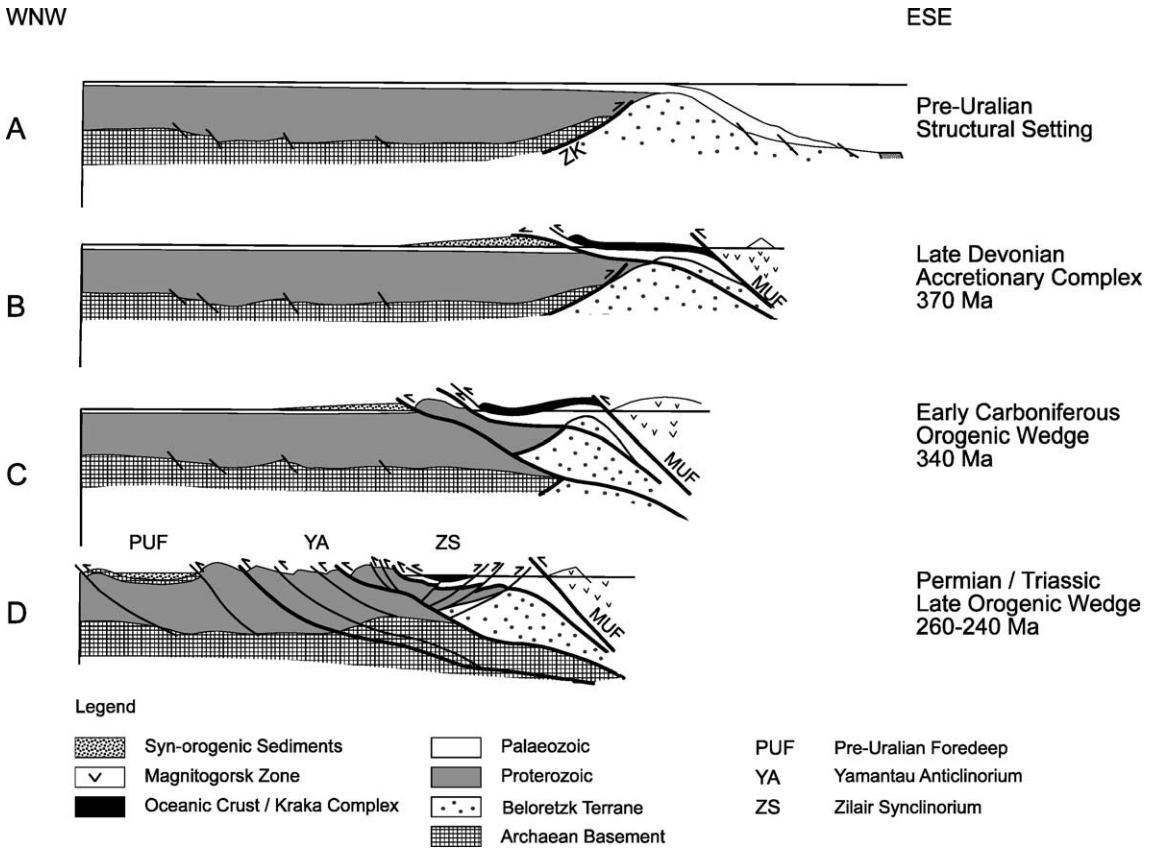


Fig. 5. Sketch of the structural evolution of the western fold-and-thrust belt in the southern Uralides (no scale) (Giese, 2000; Giese et al., 1999). (A) Pre-Uralian structural setting, (B) Upper Devonian accretionary complex, (C) Lower Carboniferous orogenic wedge, (D) Permian late orogenic wedge.

al., 1997, 2000; Brown and Spadea, 1999). This is based on radiometric ages of about 385–365 Ma for the HP metamorphism in the Maksyutovo complex and the onset of the Zilair flysch sedimentation at the beginning of the Famennian, i.e. 370 Ma (Matte et al., 1993; Shatsky et al., 1997; Hetzel et al., 1998; Brown et al., 1998, 2000, 2001; Beane and Connelly, 2000; Remaine et al., 2000; Glodny et al., 2002). Tectonic accretion of oceanic crust and basin-and-slope units resulted in an accretion complex, which prograded towards the NW and moved onto the EEC (Fig. 5B). Continuous NW–SE-directed convergence and continental subduction resulted in the formation of an early tectonic wedge at about 340 Ma (Fig. 5C). The Neoproterozoic metamorphic basement block moved onto the EEC, exhuming the accretionary complex. The Zilair synclinorium and the Yamantau anticlinorium are formed as hanging wall structures when the basal detachment cut into the former Mesoproterozoic to Neoproterozoic basin (Fig. 5D). The main shortening of the Uralian deformation occurred during these first two stages in the Middle to Upper Devonian and Lower Carboniferous. The orogenic evolution in the SW Uralides ended in the Upper Permian to Lower Triassic, with a final phase of E–W-directed shortening (Fig. 5D). The orogenic wedge propagated further to the west, creating the western fold-and-thrust belt partly by reactivation and inversion of Mesoproterozoic to Neoproterozoic normal faults (Brown et al., 1999; Giese, 2000). Tectonic transport of the hanging wall was directed towards the west. For the tectonic wedge, the reconstruction from balanced sections indicates 15–20% of tectonic shortening, while for the Pre-Uralian Foredeep 8–10% of tectonic shortening was estimated (Giese, 2000).

## 3. Sample description and analytical methods

Along the road from Archangelskoje to Beloretzk (AC-TS'96 transect), 48 samples were collected from a variety of stratigraphic levels, including Proterozoic basement as well as Ordovician to Permian sedimentary rocks (Fig. 4). Eight samples of Mesoproterozoic to Neoproterozoic dikes and two Ordovician volcanic rocks were included. Only 32 samples revealed a sufficient amount of apatite for FT dating (Fig. 4 and Table 1). Apatite grain mounts were obtained using standard sample preparation techniques (Grist and Ravenhurst, 1992a,b; Glasmacher et al., 1998). FT ages were determined using the external detector method (Wagner and Van den haute, 1992). Samples were irradiated at the Thetis reactor (channel no. 16), Gent, in the presence of three glass neutron dosimeter (CN5) of known uranium content and Fish Canyon, Durango and Mt. Dromedary apatite age standards. Apatite was etched in 2.5% $HNO_3$ for 30 s at 23 °C and detection mica in 40% HF for 20 min at 23 °C. Area densities (tracks/cm$^2$) of spontaneous and induced fission tracks were measured using Leica Aristomat (Heidelberg) optical microscopes with magnification of 1600× dry objective. The Merzhaeuser stage of the Leica microscope is controlled by the FT STAge System of Trevor Dumitru.

FT pooled and weighted mean ages ($\pm 1\ \sigma$ error) were calculated by applying the IUGS recommended approach of Hurford and Green (1983). The ζ-value of $341 \pm 16$ a/cm$^2$ for CN5 was obtained by using Fish Canyon, Durango and Mount Dromedary apatite age standards. Radial plots were calculated and drawn with the TRACKKEY program of Dr. István Dunkl (Universität Tübingen). Confined tracks were measured with a precision of approximately $\pm 0.2$ μm at 1600× magnification using a digitising pad interfaced with a personal computer.

As described by various authors (Gleadow and Duddy, 1981; Green, 1996; Glasmacher et al., 1998 and references therein; Carlson et al., 1999), the chemical composition of apatite has a direct influence on the annealing kinetics of fission tracks. The chemical composition of apatite grains was determined using a CAMECA SX51 microprobe of the Mineralogical Institute (Universität Heidelberg) with an EDS and WDS analysing system (Table 2).

Based on the apatite FT and geological data, time–temperature paths for samples were calculated using the AFTSolve program. Ketcham et al. (2000) describe the AFTSolve program in detail. With regard to the chemical composition of the apatite grains, the thermal history was modelled using the multikinetic annealing model of Ketcham et al. (1999). Although the program attempts to find out of more than 10,000 single t–T paths those ones that best approximate the measured data (Best Fit), the primary goal of the program is to define envelopes (merit value of 0.05 and 0.5) in t–T space that contain all paths passing

Table 1
Description of samples for apatite fission track analysis and summary of FT data

| Location no. | Sample no. | Elevation of sample location (m) | Stratigraphy | Depositional age (Ma) | Lithology | $U$ (standard) (ppm) | $n$ | Spontaneous tracks | | Induced tracks | | $\chi^2$ (%) | Age ± 1 $\sigma$ (Ma) | C. T. | Mean length (standard) (μm) |
|---|---|---|---|---|---|---|---|---|---|---|---|---|---|---|---|
| | | | | | | | | $\rho_s$ | $N_s$ | $\rho_i$ | $N_i$ | | | | |
| 1 | 2101 | 340 | Perm. (Artinskian) $P_1a_1$ | ~ 265 | Conglomerate | 12 (12) | 24 | 17.84 | 1604 | 15.47 | 1391 | 20 | 361 (21) | 124 | 12.7 (1.5) |
| 18 | 2107 | 340 | Perm. (Artinskian) $P_1a_1$ | ~ 265 | Conglomerate | 9 (7) | 30 | 17.50 | 1585 | 13.64 | 1235 | 31 | 407 (24) | 90 | 12.7 (1.2) |
| 21 | 2109 | 340 | Perm. (Artinskian) $P_1a_1$ | ~ 265 | Conglomerate | 14 (14) | 25 | 21.63 | 2144 | 21.16 | 2097 | 16 | 321 (18) | 108 | 13.5 (1.0) |
| 35 * | 2114 | 400 | Vend. (Basa) Vbs Top | ~ 580 | Sandstone | 19 (11) | 20 | 26.85 | 1543 | 27.06 | 1555 | 99 | 312 (18) | 101 | 12.8 (1.5) |
| 35 | 2117 | 400 | Vend. (Basa) Vbs Mid. | ~ 590 | Sandstone | 21 (17) | 21 | 33.62 | 2129 | 33.53 | 2123 | 87 | 315 (18) | 109 | 12.7 (1.1) |
| 37 | 2119 | 400 | Up. Riph. (Uk) $Uk_1$ | ~ 690 | Sandstone | 19 (19) | 24 | 28.46 | 1443 | 26.05 | 1321 | 14 | 348 (21) | 15 | 12.5 (1.0) |
| 56 | 2127 | 400 | Vend. (Kukkarauk) Vkk | ~ 560 | Sandstone | 4 (3) | 11 | 5.42 | 238 | 5.74 | 252 | 100 | 297 (30) | – | – |
| 58 | 2170 | 480 | Vend. (Zigan) | ~ 550 | Sandstone | 16 (14) | 20 | 22.36 | 1240 | 23.73 | 1316 | 99 | 297 (18) | 58 | 12.8 (1.2) |
| 60 | 2131 | 500 | Vend. (Zigan) | ~ 550 | Sandstone | 15 (12) | 21 | 21.52 | 1497 | 22.72 | 1580 | 81 | 298 (18) | 69 | 12.8 (1.0) |
| 103 | 2176 | 520 | L. Dev. Emsian | ~ 390 | Sandstone | 9 (16) | 19 | 14.11 | 824 | 13.73 | 802 | Failed | 288 (16) | – | – |
| 108 | 2134 | – | L. Dev. Emsian | ~ 390 | Sandstone | 23 (19) | 30 | 37.71 | 2158 | 8.74 | 500 | Failed | 265 (23) | 70 | 10.8 (1.8) |
| 69 | 2135 | 580 | U. Riph. (Zilmerdak) $R_3Zl_1$ | ~ 1000 | Conglomerate | 15 (16) | 20 | 20.17 | 1517 | 20.51 | 543 | 99 | 309 (18) | 110 | 12.8 (1.3) |
| 72 | 2138 | 620 | U. Riph. (Zilmerdak) $R_3Zl_1$ | ~ 1000 | Conglomerate | 24 (10) | 4 | 36.17 | 248 | 35.01 | 240 | 80 | 329 (34) | – | – |
| 82 | 2146 | 660 | U. Riph. (Zilmerdak) $R_3Zl_2$ | ~ 1000 | Sandstone | 29 (22) | 20 | 31.00 | 983 | 44.82 | 1421 | 100 | 219 (14) | 25 | 13.1 (1.3) |
| 84 | 2147 | 660 | U. Riph. (Zilmerdak) $R_3Zl_3$ | ~ 1000 | Conglomerate | 16 (10) | 5 | 17.92 | 320 | 22.91 | 409 | 99 | 247 (22) | 16 | 12.4 (1.9) |
| 85 | 2148 | 650 | U. Riph. (Zilmerdak) $R_3Zl_4$ | ~ 1000 | Sandstone | 21 (14) | 21 | 24.42 | 1632 | 31.75 | 2122 | 100 | 243 (14) | 83 | 12.7 (1.1) |
| 309 | 2160 | 400 | U. Riph. (Zilmerdak) $R_3Zl_3$ | ~ 1000 | Sandstone | 14 (10) | 10 | 15.25 | 480 | 20.18 | 635 | 99 | 239 (18) | 12 | 12.6 (1.2) |
| 606 | 2167 | 520 | U. Riph. (Avzyan) $Av_1^2$ | ~ 1100 | Sandstone | 26 (31) | 10 | 12.45 | 214 | 9.89 | 170 | 96 | 111 (12) | 9 | 12.2 (1.2) |
| 631 | 2211 | 580 | L. Riph. (Suran 3) $R_1sr_3$ | ~ 1400 | Sandstone | 30 (25) | 16 | 14.01 | 558 | 11.62 | 463 | 96 | 106 (8) | 7 | 12.9 (1.5) |
| 625 | 2208 | 600 | L. Riph. (Yusha 2) $R_1js_2$ | ~ 1400 | Sandstone | 60 (25) | 20 | 61.96 | 1823 | 24.61 | 724 | 99 | 219 (14) | 95 | 12.4 (1.5) |
| 623 | 2204 | 620 | L. Riph. (Yusha 2) $R_1js_2$ | ~ 1400 | Sandstone | 12 (15) | 7 | 6.33 | 128 | 2.67 | 54 | 100 | 199 (33) | 7 | 12.8 (1.3) |
| 622 | 2202 | 640 | L. Riph. (Suran 3) $R_1sr_3$ | ~ 1400 | Sandstone | 15 (16) | 20 | 10.91 | 373 | 5.44 | 186 | 100 | 175 (18) | – | – |
| 617 | 2198 | 600 | L. Riph. (Suran 4) $R_1sr_4$ | ~ 1400 | Sandstone | 25 (21) | 20 | 12.60 | 400 | 8.60 | 273 | 100 | 123 (11) | 47 | 12.3 (1.8) |
| 616 | 2225 | 650 | Precambrian | u.k. | Andesite dike | 5 (2) | 20 | 5.92 | 307 | 2.22 | 115 | 100 | 232 (28) | 22 | 12.6 (1.5) |
| 214 | 2194 | 600 | Precambrian | u.k. | Diabase dike | 3 (1) | 30 | 2.92 | 311 | 3.70 | 394 | 100 | 251 (22) | – | – |
| 109 | 2188 | 480 | Precambrian | u.k. | Diabase dike | 3 (1) | 25 | 2.81 | 208 | 3.66 | 271 | 100 | 244 (25) | – | – |
| 154 | 2174 | 450 | Mid. Devonian | ~ 380 | Sandstone | 11 (7) | 14 | 10.90 | 321 | 4.42 | 130 | 100 | 207 (24) | 16 | 12.0 (1.4) |
| 351 | 2172 | 450 | Carboniferous | u.k. | Metagreywacke | 18 (17) | 21 | 19.12 | 1084 | 7.72 | 438 | 100 | 216 (16) | 103 | 12.5 (1.4) |
| 360 | 2182 | 450 | Carboniferous | u.k. | Sandstone | 3 (1) | 15 | 2.60 | 130 | 1.08 | 54 | 100 | 202 (34) | 3 | 12.9 (1.9) |
| 189 | 2183 | 500 | Ordovician | u.k. | Volcanic rocks | 2 (1) | 6 | 1.89 | 43 | 0.75 | 17 | 99 | 220 (64) | – | – |
| T4 | 2232 | 560 | Vendian | u.k. | Sandstone | 16 (12) | 20 | 19.93 | 1286 | 5.80 | 374 | 100 | 286 (21) | 76 | 12.1 (1.7) |
| T5 | 2233 | 560 | Ordovician | u.k. | Sandstone | 16 (6) | 4 | 26.60 | 238 | 7.49 | 67 | 97 | 307 (45) | 4 | 13.6 (1.6) |

Sample locations are given by location numbers. $n$ = number of counted apatite grains, $\rho_s$ = density of spontaneous tracks ( $\times 10^6$/cm$^2$), $N_s$ = number of spontaneous tracks, $\rho_i$ = density of induced tracks ( $\times 10^6$/cm$^2$), $N_i$ = number of induced tracks, Nd = 30,000 tracks counted on CN5, u.k. = unknown, C.T. = confined tracks. $\chi^2$ (%) probability of greater values. Ages [361 (21)] are calculated as pooled ages using a $\zeta$-value of 341 ± 16 a/cm$^2$. Ages of two samples, which failed $\chi^2$ test, were calculated as weighted mean ages. Samples with more than 50 measured confined tracks were used for thermal modelling.

Table 2
Microprobe analyses of apatite grains from different sample locations and stratigraphic positions described as average with standard deviation

| Sample no. | 2101 | 2107 | 2109 | 2114 | 2117 | 2119 | 2127 | 2170 | 2131 | 2176 |
|---|---|---|---|---|---|---|---|---|---|---|
| *n* | 25 | 28 | 25 | 19 | 18 | 30 | 8 | 17 | 20 | 15 |
| Stratigraphy | Perm. | Perm. | Perm. | Vend. | Vend. | Vend. | Vend. | Vend. | Vend. | Dev. |
| $P_2O_5$ | 41.31 (79) | 41.63 (61) | 41.18 (49) | 41.62 (36) | 41.99 (60) | 41.43 (54) | 41.47 (44) | 42.06 (55) | 41.42 (1.74) | 41.83 (26) |
| $SiO_2$ | 0.24 (22) | 0.18 (13) | 0.16 (9) | 0.23 (17) | 0.14 (10) | 0.11 (6) | 0.24 (5) | 0.22 (25) | 0.08 (11) | 0.06 (7) |
| FeO | 0.14 (8) | 0.13 (8) | 0.15 (9) | 0.10 (8) | 0.08 (9) | 0.04 (3) | 0.16 (8) | 0.09 (6) | 0.05 (5) | 0.09 (10) |
| CaO | 55.65 (61) | 55.64 (42) | 55.77 (77) | 55.86 (44) | 55.39 (49) | 56.04 (39) | 55.63 (41) | 55.50 (55) | 56.05 (46) | 55.65 (38) |
| MnO | 0.11 (4) | 0.11 (5) | 0.13 (7) | 0.11 (7) | 0.07 (4) | 0.06 (3) | 0.04 (1) | 0.11 (6) | 0.10 (7) | 0.03 (2) |
| SrO | 0.28 (41) | 0.13 (17) | 0.13 (12) | 0.08 (6) | 0.22 (40) | 0.05 (4) | 0.36 (26) | 0.07 (14) | 0.05 (3) | 0.31 (41) |
| $Na_2O$ | 0.14 (10) | 0.10 (5) | 0.10 (7) | 0.07 (4) | 0.08 (7) | 0.04 (3) | 0.04 (2) | 0.07 (6) | 0.05 (4) | 0.06 (4) |
| $H_2O$ | 0.61 (16) | 0.77 (21) | 0.58 (17) | 0.44 (16) | 0.38 (17) | 0.26 (18) | 0.35 (32) | 0.47 (34) | 0.38 (17) | 0.25 (17) |
| F | 2.27 (35) | 1.90 (50) | 2.17 (53) | 2.57 (46) | 2.79 (49) | 3.10 (47) | 3.00 (68) | 2.67 (76) | 2.94 (38) | 3.15 (31) |
| Cl | 0.35 (22) | 0.45 (35) | 0.63 (56) | 0.47 (43) | 0.32 (46) | 0.18 (23) | 0.02 (2) | 0.23 (22) | 0.0 (4) | 0.15 (28) |
| Sum | 101.09 (67) | 101.04 (68) | 101.01 (72) | 101.56 (18) | 101.47 (58) | 101.32 (52) | 101.31 (29) | 101.48 (37) | 101.15 (1.58) | 101.58 (7) |

| Sample no. | 2134 | 2135 | 2146 | 2147 | 2148 | 2160 | 2167 | 2211 | 2208 | 2204 |
|---|---|---|---|---|---|---|---|---|---|---|
| *n* | 28 | 17 | 19 | 5 | 20 | 7 | 10 | 10 | 19 | 5 |
| Stratigraphy | Dev. | Up. Riph. | Up. Riph. | Up. Riph. | Up. Riph. | Up. Riph. | Up. Riph. | L. Riph. | L. Riph. | L. Riph. |
| $P_2O_5$ | 42.18 (40) | 41.73 (28) | 41.52 (57) | 41.77 (12) | 41.81 (53) | 41.15 (67) | 42.12 (46) | 41.92 (31) | 41.93 (32) | 42.25 (45) |
| $SiO_2$ | 0.14 (14) | 0.19 (8) | 0.20 (14) | 0.07 (2) | 0.17 (21) | 0.19 (12) | 0.12 (12) | 0.13 (10) | 0.26 (14) | 0.06 (5) |
| FeO | 0.04 (5) | 0.17 (13) | 0.04 (3) | 0.02 (1) | 0.04 (4) | 0.03 (1) | 0.08 (13) | 0.05 (3) | 0.03 (2) | 0.02 (2) |
| CaO | 55.66 (28) | 55.70 (29) | 55.87 (27) | 56.07 (15) | 55.93 (44) | 56.12 (40) | 55.74 (48) | 55.83 (27) | 55.70 (32) | 55.54 (15) |
| MnO | 0.06 (4) | 0.07 (4) | 0.06 (3) | 0.05 (2) | 0.04 (1) | 0.04 (1) | 0.03 (2) | 0.06 (3) | 0.06 (3) | 0.08 (8) |
| SrO | 0.02 (2) | 0.04 (3) | 0.07 (7) | 0.03 (3) | 0.03 (3) | 0.02 (1) | 0.07 (15) | 0.05 (5) | 0.03 (2) | 0.04 (3) |
| $Na_2O$ | 0.05 (4) | 0.05 (4) | 0.03 (3) | 0.04 (2) | 0.03 (3) | 0.03 (3) | 0.02 (2) | 0.02 (2) | 0.03 (3) | 0.06 (5) |
| $H_2O$ | 0.42 (19) | 0.21 (15) | 0.29 (21) | 0.23 (11) | 0.34 (14) | 0.34 (18) | 0.41 (28) | 0.20 (19) | 0.20 (5) | 0.21 (24) |
| F | 2.81 (44) | 3.24 (33) | 3.05 (54) | 3.23 (27) | 2.98 (29) | 3.00 (36) | 2.90 (57) | 3.34 (39) | 3.33 (12) | 3.33 (49) |
| Cl | 0.15 (16) | 0.15 (12) | 0.18 (26) | 0.08 (9) | 0.12 (8) | 0.04 (4) | 0.02 (3) | 0.02 (1) | 0.04 (3) | 0.02 (1) |
| Sum | 101.54 (27) | 101.55 (7) | 101.31 (52) | 101.58 (6) | 101.49 (59) | 100.96 (1.01) | 101.52 (37) | 101.61 (3) | 101.61 (1) | 101.61 (4) |

| Sample no. | 2202 | 2198 | 2225 | 2174 | 2172 | 2182 | 2183 | 2232 |
|---|---|---|---|---|---|---|---|---|
| *n* | 19 | 8 | 14 | 10 | 21 | 8 | 5 | 20 |
| Stratigraphy | L. Riph. | L. Riph. | Precamb. | Dev. | Carb. | Carb. | Ord. | Vend. |
| $P_2O_5$ | 42.28 (26) | 41.99 (72) | 41.39 (37) | 42.23 (37) | 42.15 (47) | 42.76 (54) | 41.95 (39) | 41.96 (56) |
| $SiO_2$ | 0.10 (11) | 0.55 (1.72) | 0.68 (82) | 0.08 (8) | 0.24 (14) | 0.13 (12) | 0.09 (19) | 0.23 (49) |
| FeO | 0.03 (3) | 0.05 (3) | 0.30 (10) | 0.03 (2) | 0.16 (9) | 0.28 (67) | 0.03 (2) | 0.03 (2) |
| CaO | 55.55 (27) | 55.17 (1.11) | 55.05 (59) | 55.57 (28) | 55.03 (50) | 54.95 (65) | 56.19 (28) | 55.53 (51) |
| MnO | 0.04 (6) | 0.06 (3) | 0.07 (2) | 0.09 (5) | 0.09 (5) | 0.05 (3) | 0.05 (6) | 0.05 (4) |
| SrO | 0.04 (2) | 0.04 (3) | 0.13 (2) | 0.06 (10) | 0.17 (18) | 0.06 (5) | 0.04 (3) | 0.11 (14) |
| $Na_2O$ | 0.03 (3) | 0.02 (3) | 0.03 (3) | 0.07 (3) | 0.12 (6) | 0.05 (3) | 0.06 (6) | 0.05 (12) |
| $H_2O$ | 0.21 (17) | 0.06 (5) | 0.03 (2) | 0.34 (21) | 0.39 (11) | 0.40 (45) | 0.58 (19) | 0.17 (7) |
| F | 3.31 (35) | 3.64 (11) | 3.67 (6) | 3.01 (46) | 2.84 (25) | 2.96 (92) | 2.55 (40) | 3.40 (14) |
| Cl | 0.03 (1) | 0.03 (2) | 0.06 (1) | 0.11 (10) | 0.22 (14) | 0.00 | 0.01 | 0.02 (3) |
| Sum | 101.61 (2) | 101.59 (1) | 101.40 (21) | 101.58 (25) | 101.41 (50) | 101.64 (6) | 101.55 (22) | 101.55 (21) |

Operating parameters: 10 μm beam size, 15 kV acceleration voltage, 20 nA current. Fluor: 20 s counting time. Detection limit: major elements 0.1 wt.%, trace elements 0.01 wt.%. Standards are Durango apatite (P + F), wollastonite (Si + Ca), hematite (Fe), rhodonite (Mn), periclase (Mg), albite (Na), coelestine (Sr) and scapolite (Cl). Calculation of OH content by F + Cl + OH = 2.

baseline statistical criteria and being conform to user-entered geological constraints.

## 4. Results

### 4.1. Fission track age

In general, the apatite fission track pooled age pattern of the western fold-and-thrust belt along the AC-TS'96 transect is very variable. Ages range from 106 ± 8 to 407 ± 24 Ma (Table 1 and Fig. 4). With the exception of the samples of the Pre-Uralian Foredeep, all ages are significantly younger than the sedimentation or intrusion age. Applying the known tectonic subdivisions of the western fold-and-thrust belt as described by Giese et al. (1999), the data are organized in the following manner.

Three Lower Permian conglomerates (flysch deposit nos. 1, 18 and 21) of the Pre-Uralian Foredeep revealed pooled fission track ages ranging between 321 ± 18 and 407 ± 24 Ma that are older than the sedimentation age of about 265 Ma (Table 1 and Fig. 4). The old ages and the single grain age distribution (Fig. 6) indicate that the Lower Permian at the eastern rim of the Pre-Uralian Foredeep was never heated above 120 °C after deposition.

Vendian and Upper Riphean siliciclastic units (nos. 35*, 35, 37, 56, 58, 60, 69 and 72) of the Ala-Tau anticlinorium and the western part of the Inzer synclinorium are characterized by fission track ages between 297 ± 18 and 315 ± 18 Ma. One slightly older age (348 ± 21 Ma) was revealed in the hanging wall of the Ala-Tau thrust (Figs. 4 and 7). West of the Zilmerdak thrust, fission track ages of two Lower Devonian sandstones (nos. 103 and 108), which discordantly overlie Vendian flysch deposits, failed the $\chi^2$ test. Single apatite grains show a wide spread in age (Fig. 6). The oldest single grain ages with the lowest 1 $\sigma$ error are in the range of about 550 Ma. The weighted mean ages of the two Lower Devonian samples are 288 ± 16 and 265 ± 23 Ma, respectively. This young weighted mean age clearly indicates that more grains have younger ages with smaller error. The Lower Devonian sample (no. 103, Fig. 4) that was taken along the AC-TS'96 transect revealed a similar age than the underlying Vendian sandstones and conglomerates.

In the eastern Inzer synclinorium, east of an unnamed fault, the pooled fission track ages of Upper Riphean sandstones (nos. 82, 84, 85 and 309) are significantly younger and range from 219 ± 14 to 247 ± 22 Ma (Figs. 3, 4 and 7). Similar ages (from 232 ± 28 to 251 ± 22 Ma) were revealed from an andesite dike (no. 616) and two diabase dikes (nos. 214 and 109) in the Beloretzk Terrane. These dikes are interpreted to be of Precambrian intrusion age (Alekseyev, 1984).

In the Yamantau anticlinorium, east of an unnamed thrust, fission track ages of Lower Riphean siliciclastic units (nos. 625, 623 and 622) are getting younger from west to east (from 219 ± 14 to 175 ± 18 Ma) (Figs. 3 and 4). These samples are bracketed by two faults, the east-dipping thrust in the west and the west-dipping Zuratkul fault in the east. Therefore, the change in age might be related to differential tectonic movement of the crustal block.

Further to the east, pooled fission track ages of Palaeozoic siliciclastic units (nos. 360, 154, 351 and 189) of the Zilair synclinorium are similar (from 202 ± 34 to 216 ± 16 Ma) to those of the eastern Yamantau anticlinorium (Fig. 4). Both areas might have experienced a similar tectonothermal evolution. Furthermore, the same ages of samples from different tectonic units in the Zilair synclinorium indicate that the Timirovo thrust sheet, the Zilair nappe and the Uzyan nappe were exhumed at the same time (Figs. 3 and 4). Pooled fission track ages of a Vendian (no. T4, 286 ± 21 Ma) and an Ordovician sandstone (no. T5, 307 ± 45 Ma) from the Tirlyan synclinorium north of the Zilair synclinorium are significantly older but similar in age as those of the Ala-Tau anticlinorium in the west. These ages indicate that the Tirlyan synclinorium was exhumed earlier than the Zilair synclinorium.

The youngest pooled fission track ages (nos. 606, 617 and 631) are in the range between 106 ± 8 and 123 ± 11 Ma. They are all located in the Yamantau anticlinorium or the western part of the Beloretzk Terrane close to W–E trending normal faults and NW–SE trending thrusts (Figs. 3 and 4). The NE–SW trending thrusts belong to the regional thrust system of the western fold-and-thrust belt. Those thrusts that dip to the east are related to the Uralian deformation, whereas those that dip to the west are related to the Neoproterozoic orogen. The W–E

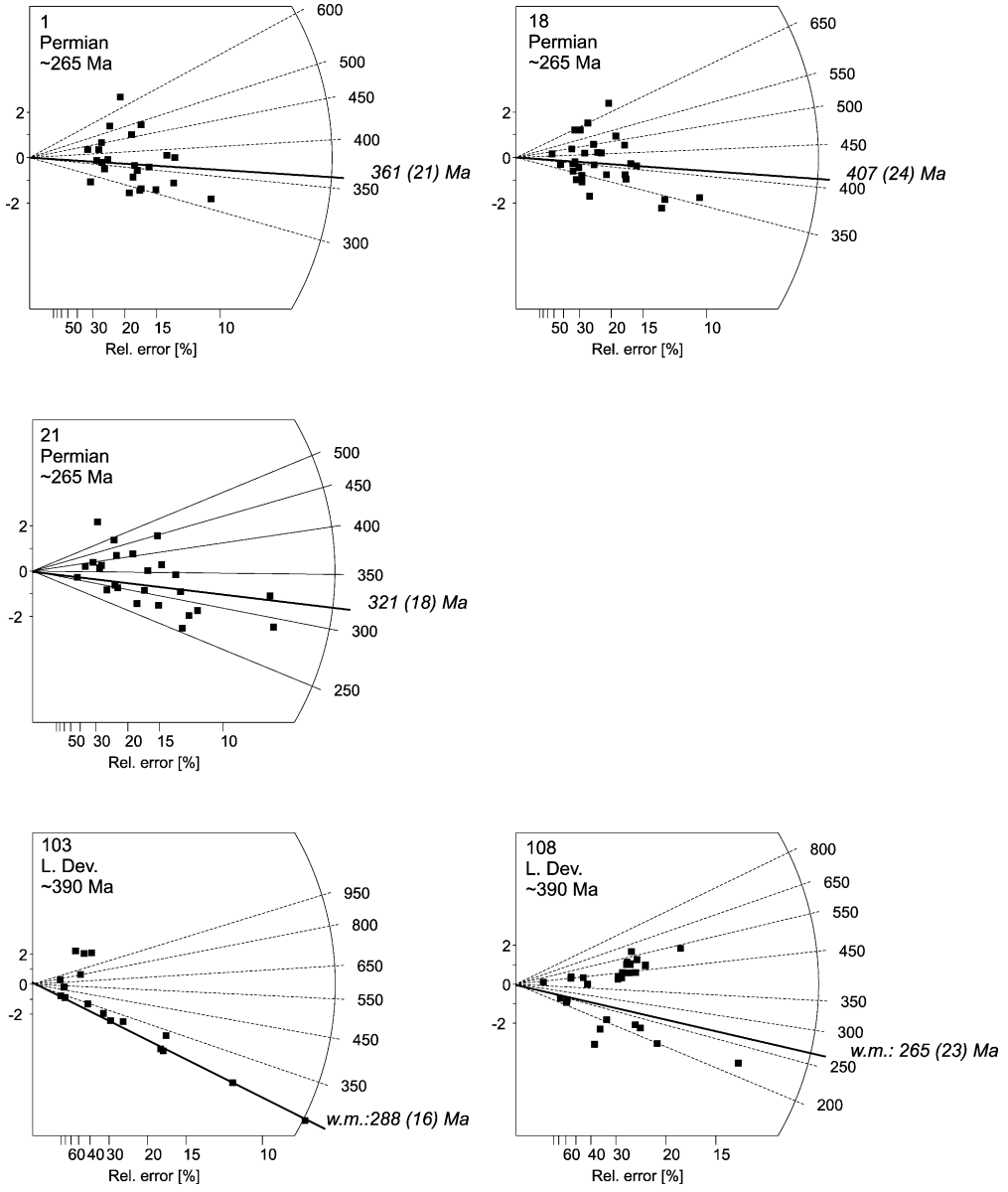


Fig. 6. Radial plots displaying apatite FT single grain ages of Permian conglomerates and samples that failed the $\chi^2$ test.

trending normal faults are of unknown age. They occur throughout the whole Bashkirian Mega-anticlinorium. The stratigraphic age of the lithologies on both sides of the faults indicate that the northern blocks were uplifted relative to the southern blocks. The young fission track ages occurring on the northern side of those normal faults can be explained by an uplifted northern side.

### 4.2. Chemical composition

To test the dependency of the single grain age distribution on the chemical variation, the chemical composition of dated apatite grains were determined for nearly all samples (Table 2). Apatite grains of Permian and Vendian sandstones and conglomerates are in general high in chlorine content of up to

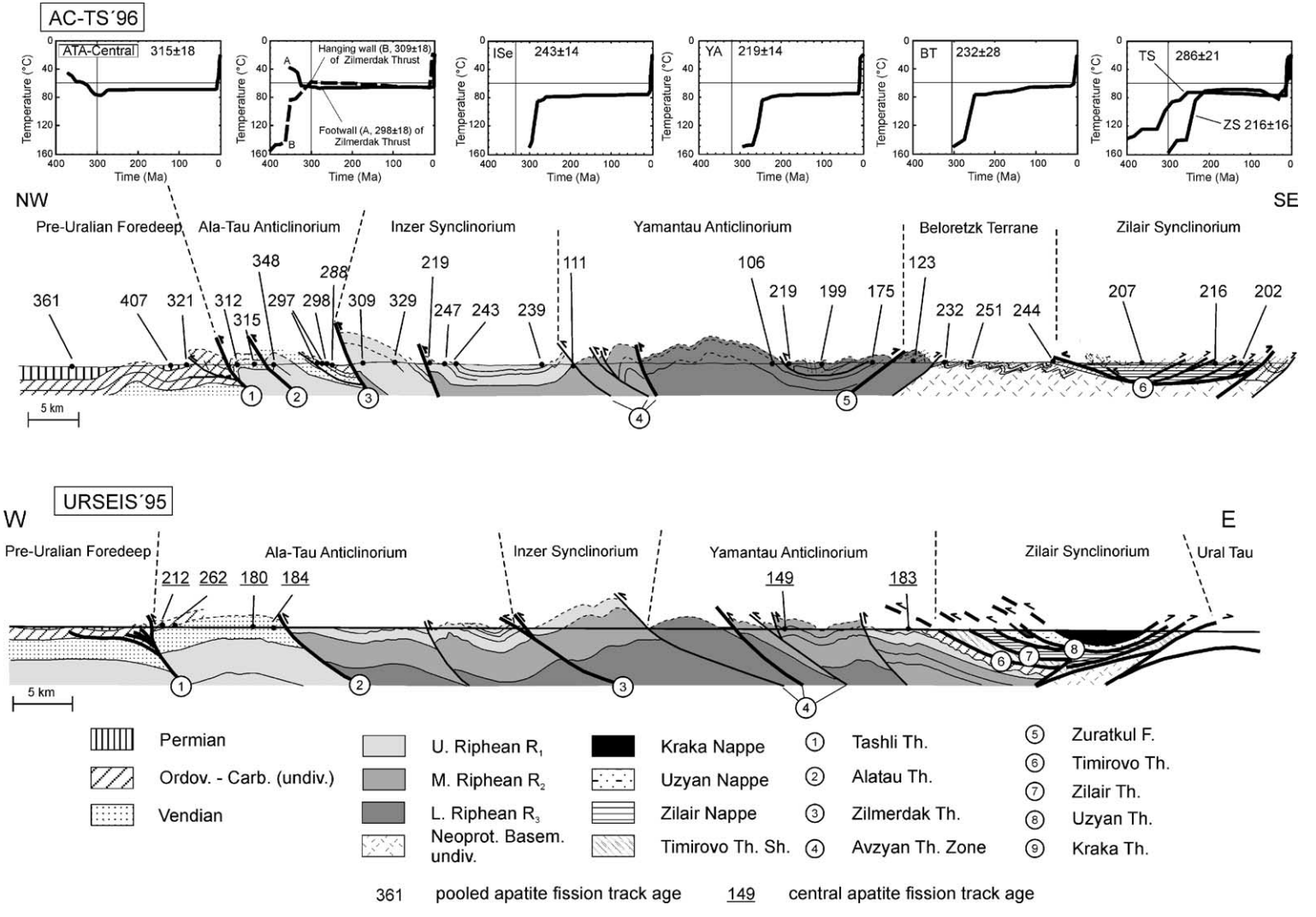


Fig. 7. Generalised WNW–ESE structural cross-section along the AC-TS'96 and URSEIS'95 transect (for location, see Figs. 1 and 3) (Giese et al., 1999). Apatite FT central ages at the URSEIS'95 transect are taken from Seward et al. (1997). Apatite FT pooled ages and time–temperature paths are described in this paper. Included are modelling results for one hanging wall sample (no. 69) and one footwall sample (no. 60) of the Zilmerdak thrust.

0.63 ± 0.56 wt.% (Table 2). The chlorine concentration is low in apatite from the Riphean sandstones and Precambrian dikes. All grains are characterized by variable iron, manganese and sodium concentrations. The strontium values show a similar distribution to those of chlorine. No correlation was found between the single grain ages and the fluorine and chlorine variation. The chlorine values were used in the modelling of the time–temperature path of the samples applying the Ketcham et al. (1999) multikinetic annealing model.

### 4.3. Track length distribution

Comparing only those samples with more than 50 confined tracks, the mean length distributions in most of the samples are very homogenous and range from 12.1 ± 1.7 to 12.8 ± 1.5 μm (Table 1 and Figs. 8–10). One Permian sample (no. 21) is characterized by a longer average track length of 13.5 ± 1.0 μm. The Lower Devonian sandstone (no. 108) that failed the $\chi^2$ test exhibits a short average track length of 10.8 ± 1.8 μm.

All distributions are unimodal with a negative skewness and a leptokurtic shape. According to Gleadow et al. (1986), a confined track length distribution of similar shape, mean length and standard deviation is typical for a slow cooling history.

### 4.4. Modelling the thermal history

The confined track length distribution together with the fission track age of samples with more than 50 confined tracks was taken to model the individual thermal history (Table 1). Those t–T paths revealed by modelling samples (nos. 82, 617 and 616) with less than 50 confined tracks must be treated very cautiously. For the modelling procedure, independent geological information about the respective region was converted into t–T constraints using the time scales of Haq and Eysinga van (1998). Little t–T information is available for the western part of the southern Urals. Therefore, the forward modelling procedure of the program was used to establish those segments of the t–T path where monotonic cooling and monotonic heating change. Such constraints were included in the inverse modelling part of the program. For most of the samples, the t–T constraints are left very wide open.

The AFTSolve® program did not find a good solution if the temperature constraints at about 30 Ma was kept below 60 °C. According to Green (1996), the model overestimates the annealing at low temperatures. Therefore, an increase in temperature at young ages is probably an artefact of the annealing model.

Vendian and Riphean samples (nos. 35*, 35, 58 and 60) of the Ala-Tau anticlinorium that show similar FT ages reveal similar t–T "best fit" paths (Figs. 7 and 8). A fast to intermediate increase of temperature during most of the Devonian and Carboniferous is indicated by all samples between Tashli and Zilmerdak thrusts. From west to east (nos. 35*–60), the maximum temperature that was reached in Upper Carboniferous decreases from about 110 to 60 °C. Despite a similar Ft age of the Upper Riphean sample (no. 69), east of the Zilmerdak thrust, the t–T path is significantly different (Fig. 9). The sample was above 120 °C until about 360 Ma. The temperature decreased in less than 10 my to 90 °C. A second decrease in temperature between 340 and 300 Ma reached a temperature of about 60 °C that kept stable until the Neogene. West of the Zilmerdak thrust, all t–T paths show a decrease in temperature to a more or less stable temperature of about 60 °C between 300 and 260 Ma. With the exception of one Vendian sample (no. 58), the temperature kept stable during the Mesozoic and most of the Cenozoic.

In the eastern Inzer synclinorium, very close to an unnamed fault, the Upper Riphean sample no. 82 revealed a slightly younger age (219 ± 14 Ma) than the other samples further to the east. The t–T path is

Fig. 8. Results of the thermal modeling with AFTSolve®, displayed in a time–temperature diagram (left) and frequency distribution (right) of measured confined track length data overlain by a calculated probability density function (best fit) of samples from the Ala-Tau anticlinorium. Modelled results in the t–T diagram are indicated by three different reliability levels (light grey envelope: all t–T paths with a merit function value of at least 0.05, middle grey envelope: all t–T paths with a merit function value of at least 0.5, black line: best fit) (Ketcham et al., 2000). Independent geological constrains are indicated by vertical brackets. Model: modelled FT age and modelled mean track length, Data: measured weighted mean FT ages and track length, Num.: number of single grains and measured track length, G.O.F.: goodness of fit. Sample is given by sample number and age of deposition.

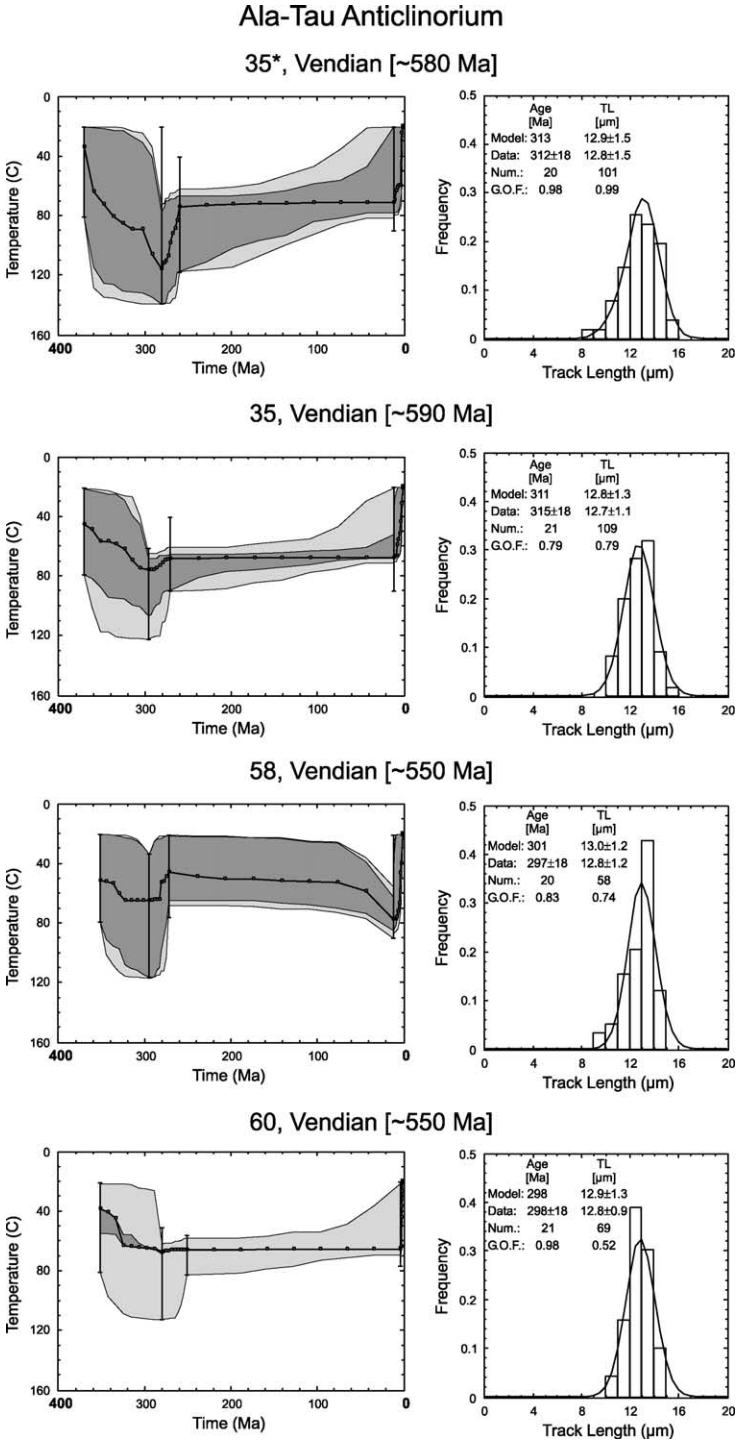
Ala-Tau Anticlinorium
35*, Vendian [~580 Ma]
Temperature (C)
Time (Ma)
Age [Ma] TL [µm]
Model: 313 12.9±1.5
Data: 312±18 12.8±1.5
Num.: 20 101
G.O.F.: 0.98 0.99
Frequency
Track Length (µm)
35, Vendian [~590 Ma]
Age [Ma] TL [µm]
Model: 311 12.8±1.3
Data: 315±18 12.7±1.1
Num.: 21 109
G.O.F.: 0.79 0.79
58, Vendian [~550 Ma]
Age [Ma] TL [µm]
Model: 301 13.0±1.2
Data: 297±18 12.8±1.2
Num.: 20 58
G.O.F.: 0.83 0.74
60, Vendian [~550 Ma]
Age [Ma] TL [µm]
Model: 298 12.9±1.3
Data: 298±18 12.8±0.9
Num.: 21 69
G.O.F.: 0.98 0.52

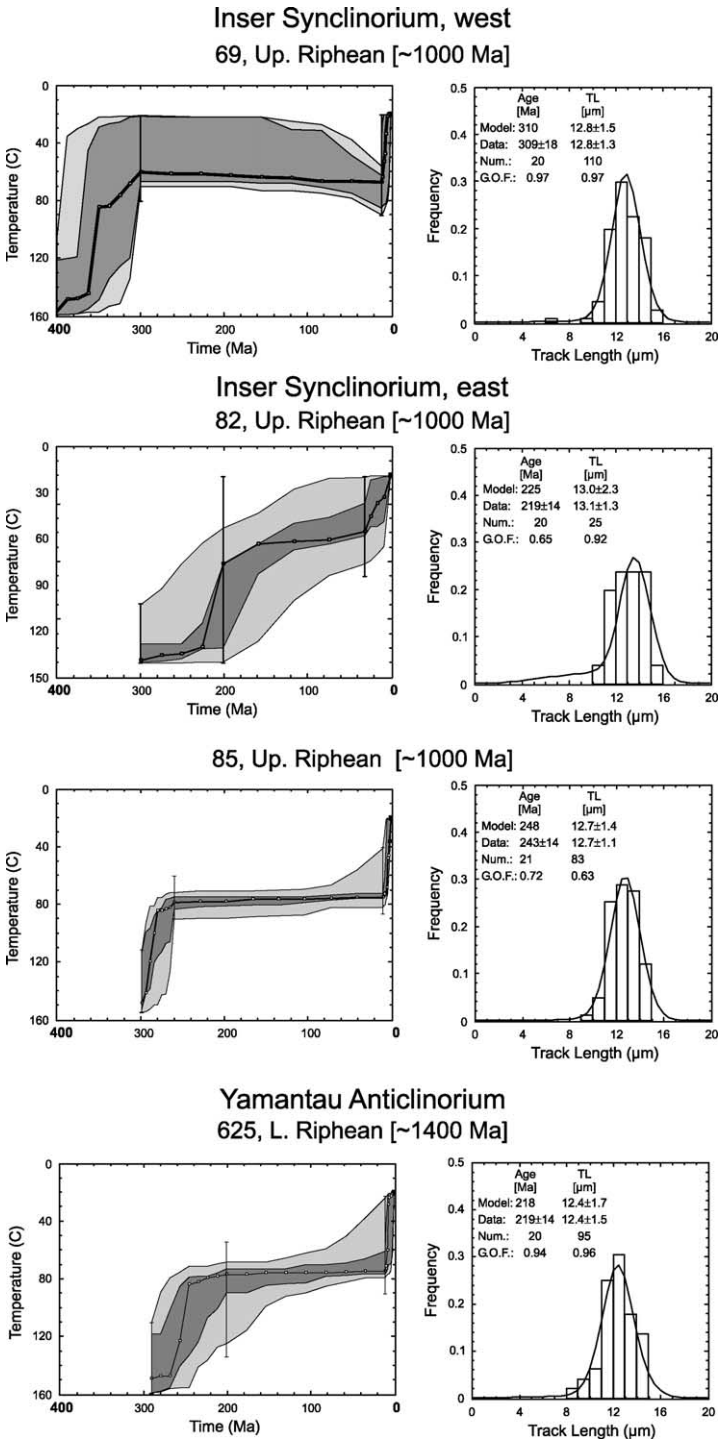


Fig. 9. Results of the thermal modelling with AFTSolve®, displayed in a time–temperature diagram (left) and frequency distribution (right) of measured confined track length data overlain by a calculated probability density function (best fit) of samples from the Inzer synclinorium and Yamantau anticlinorium. For explanation and legend, see Fig. 8.

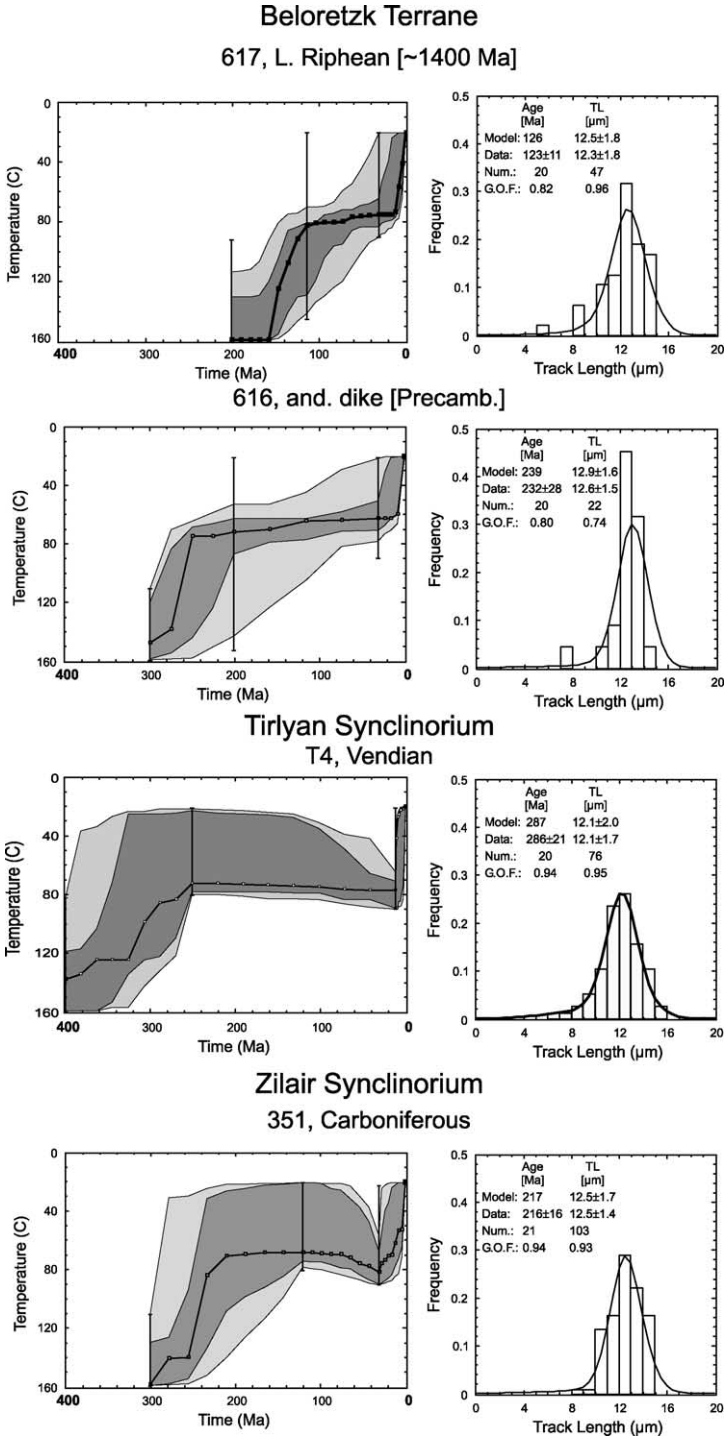


Fig. 10. Results of the thermal modelling with AFTSolve®, displayed in a time–temperature diagram (left) and frequency distribution (right) of measured confined track length data overlain by a calculated probability density function (best fit) of samples from the Beloretzk Terrane, the Tirlyan synclinorium and the Zilair synclinorium. For explanation and legend, see Fig. 8.

also different, indicating a cooling of 60 °C between 210 and 160 Ma (Fig. 9). Deformation of Early Jurassic age is known from the eastern slope of the Urals in the Chelyabinsk–Kartaly fault zone but is not recorded from the western slope. Until the Neogene, the rocks kept close to the lower limit of the PAZ. The t–T path is of very low confidence due to the few measured confined tracks. Four kilometers further to the east, the next Upper Riphean sample (no. 85, 243 ± 14 Ma) revealed a t–T path, which indicates a fast cooling by 50 °C between 300 and 280 Ma. During the Mesozoic and in Early Cenozoic, the sample remained stable at about 80 °C. The temperature of the rock decreased since the Neogene to surface temperature. The sample of the Beloretzk Terrane (no. 616) with a similar fission track age cooled by 70 °C between 280 and 260 Ma ago (Fig. 10). The Mesozoic path is similar and the model predicted that the sample remained at a temperature of about 70 °C. The t–T path is also of very low confidence due to the few measured confined tracks.

The eastern part of the Yamantau anticlinorium reveals decreasing fission track ages from west to east. The "best fit" t–T path of the Lower Riphean sample (no. 625) with the oldest age of 219 ± 14 Ma indicates a fast cooling from above 120 to about 80 °C at about 260 Ma (Fig. 9). Until the Neogene, the sample stayed nearly at the same temperature. The final decrease of temperature began at about 10 Ma ago.

An analogous t–T path is indicated for a Carboniferous metagreywacke (no. 351) of the Zilair synclinorium, which shows a similar pooled age of 216 ± 16 Ma (Fig. 10). The metagreywacke reached the upper limit of the PAZ at about 270 Ma, reached 60 °C at 220 Ma and kept at that temperature until about 30 Ma. Surface temperature was reached in the Quaternary.

In comparison, a Vendian sandstone (no. T4) of the Tirlyan synclinorium, the northern extension of the Zilair synclinorium, cooled from above 120 °C at 370 Ma, kept at about 120 °C until 330 Ma and cooled to about 70 °C at about 260 Ma ago (Fig. 10). Stable temperature conditions of about 70 °C during the Mesozoic and Lower Cenozoic were followed by a second cooling event in Neogene and Quaternary.

The time–temperature path of one of the young samples (no. 617) in the Beloretzk Terrane indicates cooling by 40 °C between 150 and 110 Ma ago (Fig. 10). During the Mesozoic, the temperature kept at about 80 °C. The final cooling to surface temperatures occurred in the Neogene.

## 5. Interpretation and discussion

The fission track data and the modelled t–T paths are best organized in relation to the tectonic subdivision of the western fold-and-thrust belt of the southern Uralides (Fig. 7). They constrain four thermotectonic episodes for the low-temperature evolution west of the MUF. Calculation of the exhumation rates considered the recent heat flow data in the Western Ural Folded zone (28–50 $mWm^{-2}$) and the Central Ural Uplift (24–43 $mWm^{-2}$) as described by Kukkonen et al. (1997). The Western Ural Folded zone extends from the Tashli thrust in the west to the Zilmerdak thrust in the east and is nearly identical with the Ala-Tau anticlinorium. The region between the Zilmerdak thrust and the Main Uralian Fault is named Central Ural Uplift and summarizes the Inzer synclinorium, the Yamantau anticlinorium, the Beloretzk Terrane, the Zilair synclinorium and the Ural-Tau. Kukkonen et al. (1997) calculated a thermal model along the Troitsk DSS transect, considering hydrological and palaeoclimatic effects as well as the radiogenetic heat production. The Troitsk DSS transect extends from west to east parallel to the URSEIS'95 transect. The thermal model indicates an average recent temperature gradient of 20 °C/km for the Ala-Tau anticlinorium and an average recent temperature gradient of 14 °C/km between Zilmerdak thrust and Main Uralian Fault. The palaeotemperature gradient might be different from the recent temperature gradient. Therefore, the exhumation rates must be treated very cautiously.

### 5.1. Devonian to carboniferous (370–295 Ma)

Siliciclastic sedimentary rocks of Lower Devonian age overlie Upper Vendian flysch deposits in the Ala-Tau anticlinorium between the Tashli and the Zilmerdak thrusts. The Ala-Tau anticlinorium is characterized by a central core of Upper Riphean sedimentary rocks and flanks of Upper Vendian flysch deposits (Fig. 7). The similarity in FT ages and t–T paths of Vendian siliciclastic units across the Ala-Tau anticlinorium indicates that the Ala-Tau region was deformed before the deposition of the Palaeozoic

sedimentary cover, which might have been caused by the Neoproterozoic orogeny (Glasmacher et al., 2001; Willner et al., 2001).

Two samples (nos. 108 and 103) of the Lower Devonian sandstone horizon revealed a wide spread in fission track single grain ages, with oldest ages of about 550 Ma. The ages indicate that those samples were only partly annealed after deposition. According to Puchkov (2000) and Kozlov et al. (1995), the Devonian to Carboniferous sequence reached a thickness of about 2500 m. Furthermore, $^{40}Ar/^{39}Ar$ spectra of microcline and orthoclase grains separated from two-mica granite pebbles of two Upper Vendian conglomerates (same location as FT sample nos. 56 and 58) indicate that the Vendian conglomerates were not heated sufficiently to reset the $^{40}Ar/^{39}Ar$ system in Palaeozoic time (Glasmacher et al., 1999, 2001). Depending on the domain size, the closure temperature of microcline can be as low as 140 °C (Lovera et al., 1991). Further to the south along the URSEIS'95 transect, Seward et al. (1997) describe that fission tracks in apatite of two Devonian samples from the western limp of the Ala-Tau anticlinorium were only partially annealed during Devonian and Carboniferous. According to Seward et al. (1997), a Vendian sample from the Ala-Tau anticline at the URSEIS'95 transects (Fig. 6) was buried during Devonian and Carboniferous to temperatures greater than 120 °C. In comparison to the FT data of the AC-TS'96, part of the Ala-Tau anticlinorium of the URSEIS'95 transect was exhumed to a greater depth.

After deposition of the Lower Palaeozoic siliciclastic units, the Ala-Tau region at the AC-TS'96 was affected by varying degrees of subsidence (Figs. 8 and 11). Whereas the t–T path of the western most Upper Vendian sample (no. 35*) reached about 110 °C for a short time interval at about 290 Ma, the t–T path of Upper Vendian samples (nos. 35, 58 and 60) further to the east are only slightly affected by temperatures of about 70 °C at about 280 Ma. The stronger increase in temperature close to the Tashli fault might be related to thicker Palaeozoic cover. Puchkov (2000) discussed the possibility of Lower Permian siliciclastic sedimentary rocks overlying the Carboniferous carbonate sequence in the western part of the Ala-Tau anticlinorium. If a temperature gradient of 20 °C/km is applied, about 5500 m of sedimentary cover would be necessary in the west and about 3500 m in the east. A sedimentary

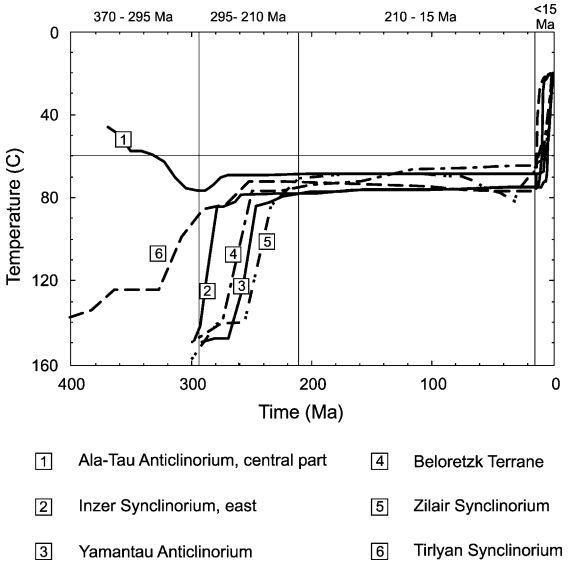


Fig. 11. Comparison of time–temperature paths of different tectonic units of the western fold-and-thrust belt, SW Uralides.

cover of more than 5000 m is not known from the region. The Devonian, Carboniferous and lowermost part of the Lower Permian sedimentary sequence reaches an overall thickness of 4000 m. Therefore, it is assumed that the palaeotemperature gradient was about 27 °C/km around the Tashli fault. It cannot be excluded that the increased heat flow might be local, has a hydrothermal thermal component and is related to the Tashli thrust. The $^{40}Ar/^{39}Ar$ spectra of microcline from an Upper Vendian conglomerate close to the Tashli fault (same location as FT sample no. 35*) indicate that the Vendian conglomerate was heated sufficiently to partly reset the $^{40}Ar/^{39}Ar$ system in Palaeozoic time (Glasmacher et al., 2001).

East of the Zilmerdak thrust, a Neoproterozoic structure, the Upper Riphean (no. 69) was above 120 °C until about 360 Ma (Figs. 7 and 12). The temperature decrease of 50 °C in less than 10 my (360–350 Ma) might be related to west-directed thrust movement along the reactivated Zilmerdak thrust that led to the exhumation of the western part of the Inzer synclinorium. In the footwall of the Zilmerdak thrust, Upper Devonian (about 370 Ma) thin bedded limestones are characterized by open, west-vergent to WNW-vergent flexural slip folding without any cleavage formation (Giese et al., 1999). The movement along the Zilmerdak thrust happened

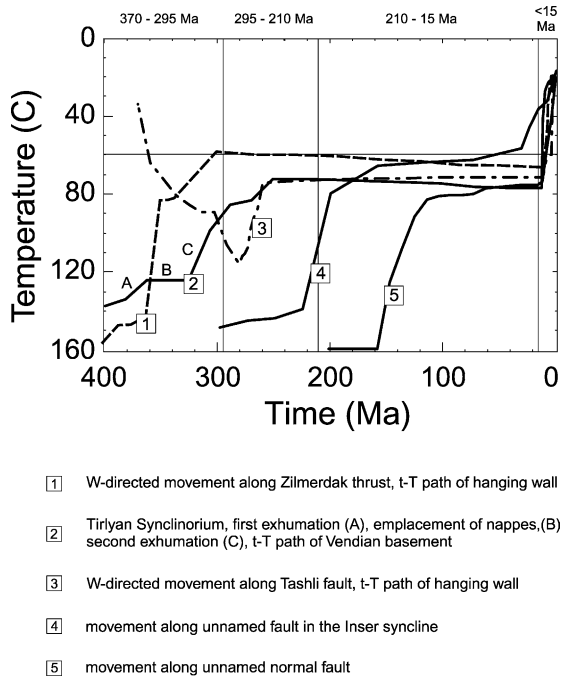


Fig. 12. Comparison of time–temperature paths caused by movement along thrusts and normal faults in the western fold-and-thrust belt, SW Uralides.

shortly after the onset of the Uralian orogeny in the east (Fig. 5) and indicates the first west-directed movement along a major thrust in the west. Assuming a temperature gradient of about 20 °C/km, movement along the Zilmerdak thrust was more than 2500 m.

A second less pronounced decrease of temperature (30 °C) between 340 and 300 Ma might indicate further exhumation of the western part of the Inzer synclinorium due to west-directed movement along the Zilmerdak thrust (Fig. 12).

At about 360 Ma, first cooling of the Vendian siliciclastic units (no. T4) of the Tirlyan synclinorium to about 120 °C might indicate the onset of the Uralian orogeny (Figs. 11 and 12). At that time, the Maksyutov complex underwent its high temperature exhumation (Leech and Stockli, 2000). The stable temperature between about 360 and 330 Ma might be related to the nappe emplacement of the Tirlyan nappe. Brown et al. (1998), Giese et al. (1999), Brown and Spadea (1999) and Giese (2000) argue that in this time range the accretionary complex in the east was west-directed tectonic transported onto the East European Craton (Fig. 5). K/Ar ages of about 340 Ma of sericite (<2 μm grain size) from slates at the base of the Zilair nappe and in the Melange below the Kraka and Tirlyan nappe are interpreted as the age of final emplacement of these nappes (Glasmacher et al., 2000). Tectonic transport of the nappes was west directed onto the autochthonous Palaeozoic units that discordantly overlie the high-grade to medium-grade metamorphic rocks of the Beloretzk Terrane. Further cooling by 30 to about 90 °C between 320 and 295 Ma might indicate the main exhumation of the Tirlyan synclinorium. Applying a temperature gradient of 14 °C/km, an exhumation rate of 0.008 mm/year can be considered. All other surrounding tectonic elements (Beloretzk Terrane and Zilair synclinorium) were above the apatite PAZ. For the same episode, Leech and Stockli (2000) describe cooling through to about 90 °C of the Maksyutov complex in the east.

### 5.2. Permian to Triassic (295–210 Ma)

During the Permian, the Pre-Uralian Foredeep was the main area of sedimentation in the western part of the southern Uralides. In the eastern part of the Pre-Uralian Foredeep, fission tracks in apatite grains from Lower Permian siliciclastic sedimentary units were partly annealed after deposition.

All tectonic units further to the east are characterized by more or less fast cooling from above 120 to about 70 °C. The Inzer synclinorium is the first tectonic unit that was exhumed at a rate of 0.03 mm/year between 290 and 280 Ma. Exhumation (0.02 mm/year) of the Beloretzk Terrane followed between 270 and 250 Ma. Shortly after (from 250 to about 240 Ma), the Yamantau anticlinorium cooled to 80 °C. The last main tectonic unit that exhumed at a rate of 0.03 mm/year between about 240 and about 230 Ma was the Zilair synclinorium. Furthermore, the same ages of samples from different tectonic units in the Zilair synclinorium indicate that the Timirovo thrust sheet, the Zilair nappe and the Uzyan nappe were exhumed simultaneously.

Between about 280 and 260 Ma, the western part of the Ala-Tau anticlinorium cooled from about 110 to 70 °C (Fig. 12). The cooling path might be related to the westward movement of the Ala-Tau anticlinorium at the Tashli thrust and therefore reflects exhumation of the western part of the Ala-Tau anticlinorium. In

the central part of the Ala-Tau anticlinorium, the temperature change due to cooling was only minor and reached a stable temperature of about 60 °C. Brown et al. (1999), Giese et al. (1999) and Giese (2000) describe a final phase of E–W-directed shortening for this episode that might have caused this cooling phase by exhumation of the different tectonic units. The exhumation rate of the different tectonic units is very similar and about 0.03 mm/year.

Along the URSEIS'95 transect, Devonian samples reached 110–120 °C in Middle Permian and cooled afterwards (Seward et al., 1997). In addition, the Vendian sample cooled during Permian and Lower Jurassic.

Leech and Stockli (2000) relate the slower monotonic cooling of the Maksyutov Complex to the post-collisional erosional degradation of the mountain belt.

### 5.3. Jurassic to Neogene (210–15 Ma)

Most T–t paths of the tectonic units indicate a stable thermal regime for the western fold-and-thrust belt of the southern Uralides between about 210 and about 15 Ma (Fig. 11). These results are consistent with a Mesozoic peneplain that was described by Shul'ts (1968) and Borisevich (1992). The temperature of about 70 °C given for that period is very close to the lower boundary of the partial annealing zone of 60 °C. Only the t–T paths of part of the Ala-Tau anticlinorium and the Zilair synclinorium indicate a period of increasing temperature in the Cretaceous, Palaeocene and Eocene (Figs. 8 and 10). No geological constraints are known from the central part of the southern Uralides that might support an increase in heat flow or a renewed subsidence of the western most part of the southern Uralides. Thin Cretaceous, Palaeocene and Eocene sedimentary deposits (< 200 m) are known from the southernmost part of the southern Uralides. Borisevich (1992) describes various terrace levels with fluvial sediments of those ages for the western slope of the southern Uralides.

The cooling path east but close to an unnamed thrust in the Inzer synclinorium indicates exhumation between 210 and 200 Ma from above 120 to 80 °C and down to 60 °C at about 160 Ma (Fig. 12). Only 8 km further to the east, the t–T path of an Upper Riphean sample (no. 85) does not show any movement at all. Therefore, it seems to be possible that the exhumation was related to local movement along the unnamed thrust. The number of confined track lengths does not justify a detailed t–T path.

The young FT ages, which occur on the northern side of W–E trending normal faults, indicate movement along these faults before about 100 Ma ago (Fig. 12). The t–T path indicates cooling of the northern side between about 150 and 120 Ma ago. Such movements would indicate a change in the tectonic regime in the southern Uralides during the Jurassic and the Cretaceous.

The t–T path of Devonian indicates a very small temperature increase from about 210 to 110 Ma and Vendian samples along the URSEIS'95 transect (Seward et al., 1997). They interpret these data as the response to burial possibly caused by Late Jurassic and Cretaceous sedimentation. Similarly, Leech and Stockli (2000) describe a small temperature increase during the Jurassic and Cretaceous for the Maksyutov Complex and related this change in t–T path to accumulation of sediments.

### 5.4. Neogene to Quaternary (~ 15 Ma to present)

Final denudation of the western fold-and-thrust belt and exhumation to the present surface probably began in the Late Tertiary (Figs. 11 and 12). However, the exact nature of this part of the t–T evolution is only poorly constrained, because the samples were already below or very close to the lower limit of the PAZ for apatite fission tracks.

## 6. Conclusion

The apatite fission track data of the western fold-and-thrust belt of the southern Uralides record various stages of the geodynamic evolution of the Uralide orogeny such as basin evolution during the Palaeozoic, synorogenic movements along major thrusts and synorogenic to postorogenic exhumation. In addition, during the Upper Jurassic and Lower Cretaceous, a change in the regional stress field is indicated.

### 6.1. Evolution of the Palaeozoic basin

The Palaeozoic sedimentary cover and the Vendian as well as Upper Riphean sedimentary units of the

Ala-Tau anticlinorium never exceed 70 °C in the east and 110 °C in the west. Thickness of the Palaeozoic sedimentary cover increased from east to west and a temperature gradient similar to the recent one (20 °C/km) would account for the FT data in the Ala-Tau anticlinorium. The Ala-Tau anticlinorium was formed during the Neoproterozoic orogeny. In the eastern part of the Pre-Uralian Foredeep, Lower Permian siliciclastic rocks never reached temperatures to completely reset the fission track age signature of the source area.

### 6.2. Movements along major thrusts

Between 360 and 350 Ma, more than 2500 m west-directed thrusting along the Zilmerdak thrust is recorded by the FT data. Reactivation of the Neoproterozoic Zilmerdak thrust is time equivalent to the onset of Uralian collision-related deformation in the east. Between 340 and 300 Ma, the second distinct movement is nearly time equivalent to the emplacement of the major nappes west of the MUF.

At the eastern rim of the Pre-Uralian Foredeep, the west-directed movement along the Tashli thrust occurred between 280 and 260 Ma.

### 6.3. Synorogenic to postorogenic exhumation

The expected east–west trend of exhumation caused by west-directed tectonic movement could not be verified by the fission track data.

First exhumation of the Vendian siliciclastic units of the Tirlyan synclinorium at about 360 Ma indicates the onset of the Uralian orogeny. At that time, the Maksyutov complex in the east underwent its high temperature exhumation. After emplacement of the Tirlyan nappe between about 360 and 330 Ma, the main exhumation (0.008 mm/year) of the Tirlyan synclinorium followed until about 295 Ma.

Exhumation of the Inzer synclinorium between 290 and 280 Ma was followed by the exhumation of the Beloretzk Terrane between 270 and 250 Ma. At nearly the same time, the western part of the Ala-Tau anticlinorium slowly exhumed (0.008 mm/year).

Shortly after, the Yamantau anticlinorium exhumed and reached a stable crustal position at about 240 Ma. The last main tectonic unit that reached a stable crustal position at 230 Ma was the Zilair synclinorium. The same ages of samples from different tectonic units in the Zilair synclinorium indicate that the Timirovo thrust sheet, the Zilair nappe and the Uzyan nappe were exhumed simultaneously. The exhumation rate of 0.03 mm/year was nearly the same in all main tectonic units.

Most of the tectonic units kept stable in the crust until the Neogene. Final denudation of the western fold-and-thrust belt and exhumation to the present surface probably began in the Late Tertiary. However, the exact nature of this exhumation is only poorly constrained, because the samples were already below or very close to the lower limit of the PAZ for apatite fission tracks system.

### 6.4. Mesozoic regional stress field

In the hanging wall of an unnamed thrust in the Inzer synclinorium, the apatite fission track system records an exhumation of the northeastern block between 210 and 160 Ma that is related to south-west-directed movement along the unnamed thrust. This deformation might be related to time-equivalent deformation known from the eastern slope of the Urals in the Chelyabinsk–Kartaly fault zone.

During the Upper Jurassic and the Cretaceous, south-directed movements along W–E trending normal faults indicate a change in the tectonic regime in the southern Uralides.

## Acknowledgements

Fieldwork in the Ural and laboratory studies were funded by the Deutsche Forschungsgemeinschaft (DFG) grants Gl182/3-1, Gl182/3-2, Gl182/3-3 and Gl182/3-4, which are gratefully acknowledged. This paper is a contribution to EUROPROBE (URALIDES). EUROPROBE is coordinated within the International Lithosphere Program and is sponsored by the European Science Foundation. The authors greatly appreciated the critical reading and the constructive comments of Prof. J-P. Burg, Dr. M. Leech and an unknown reviewer. We also express our thanks to Prof. R. Altherr and Dr. H.-P. Meyer (Mineralogisches Institut, Universität Heidelberg) for the microprobe data. As a representative of the Russian team during the fieldwork, we thank Dr.

V.N. Baryshev for his scientific and logistical help. Special thanks are given to Dr. R. Walter, Dr. U. Giese, Dr. L. Stroink and Dipl.-Geol. I. Matenaar for their help and support during fieldwork and transportation of the samples back to Germany.

## References

Alekseyev, A., 1984. Riphean and Vendian Magmatism in the Southern Urals. Nauka, Moskau 136 pp. [in Russian].

Bastida, F., Aller, J., Puchkov, V.N., Juhlin, C., Oslianski, A., 1997. A cross-section through the Zilair Nappe (southern Urals). Tectonophysics 276, 253–264.

Beane, R.J., Connelly, J.N., 2000. $^{40}Ar/^{39}Ar$, U-Pb, and Sm-Nd constraints on the timing of metamorphic events in the Maksyutov Complex, southern Ural Mountains. J. Geol. Soc. (Lond.) 157, 811–822.

Berzin, R., Oncken, O., Knapp, J.H., Pérez-Estaún, A., Hismatulin, T., Yunusov, N., Lipilin, A., 1996. Orogenic evolution of the Ural Mountains: results from an integrated seismic experiment. Science 274, 220–221.

Borisevich, D.V., 1992. Neotectonics of the Urals. Geotectonics 26, 41–47.

Brown, D., Spadea, P., 1999. Processes of forearc and accretionary complex formation during arc-continent collision in the southern Urals. Geology 27, 649–652.

Brown, D., Puchkov, V.N., Alvarez-Marron, J., Perez-Estaun, A., 1996. The structural architecture of the footwall to the Main Uralian Fault, southern Urals. Earth-Sci. Rev. 40, 125–147.

Brown, D., Alvarez-Marron, J., Perez-Estaun, A., Gorozhanina, Y., Baryshev, V., Puchkov, V., 1997. Geometric and kinematic evolution of the foreland thrust and fold belt in the southern Urals. Tectonics 16, 551–562.

Brown, D., Juhlin, C., Alvarez-Marron, J., Perez-Estaun, A., Oslianski, A., 1998. Crustal-scale structure and evolution of an arc-continent collision zone in the southern Urals, Russia. Tectonics 17, 158–171.

Brown, D., Alvarez-Marron, J., Perez-Estaun, A., Puchkov, V., Ayala, C., 1999. Basement influence on foreland thrust and fold belt development: an example from the southern Urals. Tectonophysics 308, 459–472.

Brown, D., Hetzel, R., Scarrow, J.H., 2000. Tracking the arc-continent collision subduction zone processes from high-pressure rocks in the southern Urals. J. Geol. Soc. (Lond.) 157, 901–904.

Brown, D., Alvarez-Marron, J., Perez-Estaun, A., Puchkov, V., Ayarza, P., Gorozhanina, Y., 2001. Structure and evolution of the Magnitogorsk forearc basin: identifying upper crustal processes during arc-continent collision in the southern Urals. Tectonics 20, 364–375.

Carlson, W.D., Donelick, R.A., Ketcham, R.A., 1999. Variability of apatite fission-track annealing kinetics: I. Experimental results. Am. Mineral. 84, 1213–1223.

Döring, J., Götze, H.J., 1999. The isostatic state of the southern Urals crust. Geol. Rundsch. 87, 500–510.

Echtler, H.P., Hetzel, R., 1997. Main Uralian thrust and Main Uralian normal fault: non-extensional Palaeozoic high-P rock exhumation, oblique collision and normal faulting in the southern Urals. Terra Nova 9, 158–162.

Echtler, H.P., Stiller, M., Steinhoff, F., Krawczyk, C., Suleimanov, A., Spiridonov, V., Knapp, J.H., Menshikov, Y., Alvarez-Marrón, J., Yunusov, N., 1996. Preserved collisional crustal structure of the southern Urals revealed by vibroseis profiling. Science 274, 224–226.

Giese, U., 2000. The western fold-and-thrust-belt of the southern Urals, Russia—review and perspective. N. Jb. Geol. Paläont. Abh. 218, 267–284, Stuttgart.

Giese, U., Glasmacher, U., Kozlov, V.I., Matenaar, I., Puchkov, V., Stroink, L., Walter, R., 1997. A structural cross-section across the western fold-and-thrust belt of the southern Urals. Terra Nova abst., EUG 9, Strasbourg.

Giese, U., Glasmacher, U.A., Kozlov, V., Matenaar, I., Puchkov, V., Stroink, L., Walter, R., 1999. Structural framework of the Bashkirian Anticlinorium, SW Urals. Geol. Rundsch. 87, 526–544.

Glasmacher, U.A., Matenaar, I., Pickel, W., Giese, U., Kozlov, V.I., Puchkov, V., Stroink, L., Walter, R., 1997. Incipient metamorphism of the western fold-and-thrust belt, southern Urals, Russia. Beih. z. Eur. J. Min. 9, 124.

Glasmacher, U.A., Zentilli, M., Grist, A.M., 1998. Apatite fission-track thermochronology of Palaeozoic sandstones and the Hill-Intrusion, Northern Linksrheinisches Schiefergebirge, Germany. In: van den Haute, P., de Corte, F. (Eds.), Advances in Fission-Track Geochronology. Solid Earth Sci. Libr., vol. 10. Kluwer Academic Publishing, London, pp. 151–172.

Glasmacher, U.A., Reynolds, P., Alekseev, A., Puchkov, V.N., Taylor, K., Gorozhanin, V., Walter, R., 1999. $^{40}Ar/^{39}Ar$ Thermochronology west of the Main Uralian Fault, southern Urals, Russia. Geol. Rundsch. 87, 515–525.

Glasmacher, U.A., Bauer, W., Clauer, N., Puchkov, V.N., 2000. Age of metamorphism and nappe emplacement in the western part of the southern Urals, Russia. EUROPROBE-URALIDES Workshop, München.

Glasmacher, U.A., Bauer, W., Giese, U., Reynolds, P., Kober, B., Puchkov, V.N., Stroink, L., Alekseev, A., Willner, A., 2001. The metamorphic complex of Beloretzk, SW Urals, Russia—a terrane with a polyphase Meso- to Neoproterozoic thermo-dynamic evolution. Precambrian Res. 110, 185–213.

Gleadow, A.J.W., Duddy, I.R., 1981. A natural long term track annealing experiment for apatite. Nucl. Tracks Radiat. Meas. 5, 169–174.

Gleadow, A.J.W., Duddy, I.R., Green, P.F., Lovering, J.F., 1986. Confined fission-tracks lengths in apatite: a diagnostic tool for thermal history analysis. Cont. Min. Pet. 94, 405–415.

Glodny, J., Bingen, B., Austrheim, H., Molina, J.F., Rusin, A., 2002. Precise eclogitization ages deduced from Rb/Sr mineral systematics: the Maksyutov complex, southern Urals, Russia. Geochim. Cosmochim. Acta 66/7, 1221–1235.

Green, P.F., 1996. The importance of compositional influence on fission-track annealing in apatite. Int. Workshop Fission-Track Dating (abstr. vol.), p. 43.

Grist, A.M., Ravenhurst, C.E., 1992a. Mineral separation techniques used in Dalhousie University. In: Zentilli, M., Reynolds,

P.H. (Eds.), Short Course on Low Temperature Thermochronology. Min. Assoc. Can. Short Course V 20, Appendix 2, pp. 203–209.

Grist, A.M., Ravenhurst, C.E., 1992b. A step-by-step laboratory guide to fission-track thermochronology at Dalhousie University. In: Zentilli, M., Reynolds, P.H. (Eds.), Short course on low temperature thermochronology. Min. Assoc. Can. Short Course V 20, Appendix 1, pp. 190–201.

Hamilton, W., 1970. The Uralides and the motion of the Russian and Sibirian platforms. Geol. Soc. Am. Bull. 81, 2553–2576.

Haq, B.U., Eysinga van, F.W.B., 1998. Geological Time Table, 5th edn. Elsevier, Amsterdam.

Hetzel, R., Echtler, H.P., Seifert, W., Schulte, B.A., Ivanov, K.S., 1998. Subduction- and exhumation-related fabrics in the Palaeozoic high-pressure/low-temperature Maksyutov Complex, Antingan area, southern Urals, Russia. Bull. Geol. Soc. Am. 110, 916–930.

Hurford, A.J., Green, P.F., 1983. The zeta age calibration of fission track dating. Isotope Geosci. 1, 285–317.

Ketcham, R.A., Donelick, R.A., Carlson, W.D., 1999. Variability of apatite fission-track annealing kinetics: III. Extrapolation to geological time scales. Am. Mineral. 84, 1235–1255.

Ketcham, R.A., Donelick, R.A., Donelick, M.B., 2000. AFTSolve: a program for multi-kinetic modelling of apatite fission-track data. Mineral. Soc. Am. Geol. Mater. Res. 2, 1–32.

Kozlov, V.I., 1982. Upper Riphean and Vendian in the South Ural. Nauka, Moscow, pp. 1–128 [in Russian].

Kozlov, V.I., Krasnobaev, A.A., Larionov, N.N., Maslov, A.V., Sergeeva, N.D., Ronkin, Yu.L., Bibikova, E.V., 1989. Lower Riphean of the South Urals. Nauka, Moscow, 208 pp. [in Russian].

Kozlov, V.I., Sinitsyna, Z.A., Kulagina, E.I., Pazukhin, V.N., Puchkov, V.N., Kochetkova, N.M., Abramova, A.N., Klimenko, T.V., Sergeeva, N.D., 1995. Guidebook of excursion for the Palaeozoic and Upper Precambrian sections of the Western slope of the Southern Urals and Preuralian regions. Russ. Acad. Sci., 1–165.

Kukkonen, I.T., Golovanova, I.V., Khachay, Yu.V., Druzhinin, V.S., Kosarev, A.M., Schapov, V.A., 1997. Low geothermal heat flow of the Urals fold belt—implication of low heat production, fluid circulation or palaeoclimate? Tectonophysics 276, 63–85.

Leech, M.L., 2001. Arrested orogenic development: eclogitization, delamination, and tectonic collapse. EPSL 185, 149–159.

Leech, M.L., Stockli, D.F., 2000. The late exhumation history of the ultrahigh-pressure Maksyutov Complex, south Ural Mountains, from new apatite fission-track data. Tectonics 19, 153–167.

Lovera, O.M., Richter, F.M., Harrison, T.M., 1991. The $^{40}Ar/^{39}Ar$ thermochronometry for slowly cooled samples having a distribution of diffusion domain sizes. J. Geophys. Res. 94, 17917–17935.

Maslov, A.V., Erdtmann, B.D., Ivanov, K.S., Ivanov, S.N., Krupenin, M.T., 1997. The main tectonic events, depositional history and the palaeogeography of the southern Urals during the Riphean-early Palaeozoic. Tectonophysics 276, 313–335.

Matenaar, I., Glasmacher, U.A., Pickel, W., Giese, U., Pazukhin, V.N., Kozlov, V.I., Puchkov, V.N., Stroink, L., Walter, R., 1999. Incipient metamorphism between Ufa and Beloretzk, western fold-and-thrust belt, southern Urals, Russia. Geol. Rundsch. 87, 545–560.

Matte, P., Maluski, H., Caby, R., Nicolas, A., Kepezhinskas, P., Sobolev, S., 1993. Geodynamic model and $^{39}Ar/^{40}Ar$ dating for the generation and emplacement of the high pressure (HP) metamorphic rocks in SW Urals. C. R. Acad. Sci. Paris 317 (Ser. II), 1667–1674.

Puchkov, V.N., 1988. Pre-Alpine tectonic features throughout and around the Alpine orogen. Acta Geol. Palonica, XXI, 45–65.

Puchkov, V.N., 1993. The paleo-oceanic structures of the Ural Mountains. Geotectonics 27, 184–196.

Puchkov, V.N., 1997. Structure and geodynamics of the Uralian orogen. In: Burg, J.P., Ford, M. (Eds.), Orogeny Through Time-Spec. Publ. 121, Geological Society, London, pp. 201–236.

Puchkov, V.N., 2000. Palaeogeodynamics of the Central and Southern Urals. Academy of Science, Ufa, Pauria, 145 pp.

Remaine, J., Cita, M.B., Dercourt, J., 2000. International Stratigraphic Chart and Explanatory Note, IUGS-UNESCO.

Seward, D., Pérez-Estaún, A., Puchkov, V.N., 1997. Preliminary fission-track results from the southern Urals—Sterlitamak to Magnitogorsk. Tectonophysics 276, 281–290.

Shatsky, V.S., Jagoutz, E., Koz'menko, O.A., 1997. Sm-Nd dating of the high-pressure metamorphism of the Maksyutov Complex, southern Urals. Earth Sci. Ser. 353, 285–288.

Shul'ts, S.S., 1968. Neotectonics of the Urals. Papers on Geomorphology and Neotectonics of the Urals and the Volga Region 2, 45–60, Ufa.

Steer, D.N., Knapp, J.H., Brown, L.D., Echtler, H.P., Brown, D.L., Berzin, R., 1998. Deep structure of the continental lithosphere in an unextended orogen: an explosive-source seismic reflection profile in the Urals (Urals Seismic Experiment and Integrated Studies URS-EIS 1995). Tectonics 17 (2), 143–157.

Stroink, L., Frese, K., Giese, U., Matenaar, I., Kozlov, V.I., Glasmacher, U., 1997. Compositional framework of Upper Proterozoic sandstones of the southern Urals: implications for a Pre-Uralian orogenic event. 18th IAS Heidelberg, GAEA 3, p. 324.

Wagner, G.A., Van den haute, P., 1992. Fission-Track Dating. Enke Ferdinand Verlag, Stuttgart, 285 pp.

Willner, A.P., Emolaeva, T., Stroink, L., Glasmacher, U.A., Giese, U., Puchkov, V., Kozlov, V.I., Walter, R., 2001. Contrasting provenance signals in Riphean and Vendian sandstones in the SW Urals (Russia): constraints for a change from passive to active continental margin conditions in the Neoproterozoic. Precambrian Res. 110, 215–239.

Zonenshain, L.P., Korinevsky, V.G., Kuzmin, M.I., Pechersky, D.M., Khain, V.V., Mateveenkov, V.V., 1984. Plate tectonic model of the south Urals development. Tectonophysics 109, 95–135.

Zonenshain, L.P., Kuzmin, M.I., Natapov, L.M., 1990. Uralian foldbelt. In: Page, B.M. (Ed.), Geology of the USSR: A Plate-Tectonic Synthesis. Geodyn. Ser. 21, American Geophysical Union, Washington, DC, pp. 27–54.